Laboratory Experiments on the Effects of a Variable Current Field on the Spectral Geometry of Water Waves

HENRIQUE RAPIZO

Swinburne University of Technology, Hawthorn, Victoria, Australia

TAKUJI WASEDA

Graduate School of Frontier Sciences, University of Tokyo, Kashiwa, Chiba, Japan

ALEXANDER V. BABANIN[a] AND ALESSANDRO TOFFOLI[a]

Swinburne University of Technology, Hawthorn, Victoria, Australia

(Manuscript received 3 January 2016, in final form 10 June 2016)

ABSTRACT

Laboratory experiments were performed to investigate the effects of a coflowing current field on the spectral shape of water waves. The results indicate that refraction is the main factor in modulating wave height and overall wave energy. Although the structure of the current field varies considerably, some current-induced patterns in the wave spectrum are observed. In high frequencies, the energy cascading generated by nonlinear interactions is suppressed, and the development of a spectral tail is disturbed, as a consequence of the detuning of the four-wave resonance conditions. Furthermore, the presence of currents slows the downshifting of the spectral peak. The suppression of the high-frequency energy under the influence of currents is more prominent as the spectral steepness increases. The energy suppression is also more accentuated and long-standing along the fetch when the directional spreading of waves is sufficiently broad. This result indicates that the current-induced detuning of resonant conditions is more effective when exact resonances are the primary mechanism of nonlinear interactions than when quasi resonances prevail (directionally narrow cases). Additionally, the directional analysis shows that the highly variable currents broaden the directional spreading of waves. The broadening is suggested to be related to random refraction and scattering of wave rays. The random disturbance of wavenumbers alters the nonlinear interaction conditions and weakens the energy exchanges among wave components, which is expressed in the suppression of the high-frequency energy.

1. Introduction

Wave–current interactions have been the subject of theoretical (e.g., Longuet-Higgins and Stewart 1961) and experimental studies (e.g., Lai et al. 1989) for decades. It is well known that currents can significantly affect ocean wave generation and propagation. In deep water, the refraction of waves on mesoscale current features can be significant (Rapizo et al. 2014) and be potentially responsible for energy convergence and enhanced probability of freak wave occurrence (White and Fornberg 1998). Typical conditions of fetch-limited wave growth can also be considerably affected by background currents because of the changes in the relative wind and shift of the wind stress away from the mean wind direction (Haus 2007).

Based on the radiative transfer equation (RTE), current-induced effects on waves are limited to linear refraction and energy exchanges originated from the work done by the radiation stress against the current strain (e.g., Phillips 1977), which is also linear in terms of energy. However, it has been shown that nonlinearities can play an important role in modulating the wave parameters, especially when waves steepen because of negative current gradients (e.g., Babanin et al. 2011; Moreira and Peregrine 2012). In widely used wave models based on the RTE, dissipation and nonlinear

[a] Current affiliation: University of Melbourne, Melbourne, Victoria, Australia.

Corresponding author address: Henrique Rapizo, Centre for Ocean Engineering, Science and Technology, Swinburne University of Technology, P.O. Box 218, Hawthorn, VIC 3122, Australia. E-mail: hrapizo@swin.edu.au

DOI: 10.1175/JPO-D-16-0011.1

four-wave interaction terms do not directly take into account the mean flow, since little is known about the influence of currents on these processes.

A few studies have tested the role of the dissipation and nonlinear interaction terms in spectral models under the influence of currents with interesting results. Ardhuin et al. (2012), for example, pointed out that none of the parameterizations for wave dissipation proportional to wave steepness to the fourth power are satisfactory when the dissipation is induced by adverse currents. Tamura et al. (2008) showed that the use of the discrete interaction approximation (DIA) method represents poorly the spectral transformations on mesoscale eddies. Therefore, an explicit inclusion of current in these two terms (dissipation and nonlinear interactions) must bring a considerable improvement in modeling waves at certain conditions.

Relatively little work has been done on observed wave spectral changes due to the interaction with a variable current field. Numerical simulations of unidimensional transformations have been attempted (Trulsen et al. 1990); however, field or laboratory results are scarce (Chawla and Kirby 2002), especially concerning the directional properties. By propagating over an area of strong current gradients, the wave components are expected to experience differed modification patterns, and the distribution of energy in the spectrum would be affected. It is reasonable to think that energy convergence and divergence would narrow and broaden, respectively, the directional distribution of the wave spectrum in opposing and coflowing current jets (e.g., Kenyon 1971). By perturbing the original spectral form, nonlinear interactions would act in the way to stabilize the spectral shape (e.g., Young and Van Vleder 1993; Tamura et al. 2008). This process would become more complex in highly variable current fields, and observations are needed for a more thorough understanding. Nonetheless, they are practically nonexistent.

This study aims to provide observations of the effects of a variable coflowing current on the spectral shape of water waves. Laboratory experiments were performed with background currents highly variable in space and time. The experiments were designed to investigate how a random current field affects the wave spectral geometry for different initial spectra, varying directional and nondirectional parameters. Although the current is unsteady, consistent wave spectral patterns are observed under the current influence. These transformations are shown and the possible causes discussed. In the following section, a brief theoretical background will be given. Section 3 will depict the experimental methods, including a description of the wave facility and the characteristics of the current field as well as initial wave conditions. Results and discussions are presented in section 4, separated by the main groups of experiments, which are represented by regular wave trains, unidirectional and directional irregular waves with varying steepness, and irregular waves with varying directional spreading. Concluding remarks are presented in the last section.

2. Relevant effects of currents on waves

The relevant current-induced effects on gravity waves are briefly reviewed to support the further discussions of this study. The Doppler-shifted dispersion relation, that is, $\omega - \mathbf{k}\cdot\mathbf{U} = \sigma$, considerably affects the kinematics of a propagating wave, where $\mathbf{k}$ is the wavenumber vector, ω is the absolute frequency, and σ is the frequency in a frame of reference moving with the current $\mathbf{U}$. Variations in wavenumber and, consequently, wave refraction become dependent on the spatial gradients of the current field by $d\mathbf{k}/dt = -\nabla[\mathbf{k}\cdot\mathbf{U}(x, y)]$, where $d\mathbf{k}/dt$ is the Lagrangian derivative or the rate of change of wavenumber following a wave packet. If the current field is steady, the absolute frequency ω is constant. For an unsteady current, changes in ω are dependent on local accelerations of the mean flow $\partial\mathbf{U}/\partial t$.

Under the influence of a variable current, wave energy is no longer conserved, and instead, wave action is conserved (e.g., Phillips 1977). The evolution of spectral wave action density $N(f, \theta) = E(f, \theta)/\sigma$, where $E(f, \theta)$ is spectral wave energy density, is usually expressed by the radiative transfer equation (action balance)

$$\frac{\partial N}{\partial t} + \nabla_x \cdot (\mathbf{C}_x N) + \nabla_k \cdot (\mathbf{C}_k N) = F, \tag{1}$$

where ∇_x and ∇_k are divergence operators in geographical and wavenumber space, respectively; $\mathbf{C}_x = \mathbf{c}_g + \mathbf{U}$ is the advective velocity, in which $\mathbf{c}_g$ is the intrinsic wave group velocity; and $\mathbf{C}_k = d\mathbf{k}/dt$ and F represents different forcing terms. The underlying assumption of this equation is that the current field varies in space and time at a much larger scale than the wavelength and wave period.

In spectral wave models, for example, the forcings F in (1) are subgrouped by energy input from wind, dissipation (wave breaking and bottom friction, among others), and nonlinear wave–wave interactions. The latter redistributes energy in the spectral space. Little is known about the influence of a background current field on this important process.

Nonlinear interactions are fundamental for spectral evolution and are employed by the models in terms of Hasselmann's kinetic equation (Hasselmann 1962). These resonant interactions were first pointed out by

Phillips (1960) with development of deterministic theories coming on a subsequent number of papers (Benney 1962; Longuet-Higgins 1962; Longuet-Higgins and Phillips 1962; Zakharov 1968). Third-order resonant interactions occur only when the wavenumbers meet the quadrilateral conditions

$$\begin{cases} \mathbf{k}_1 + \mathbf{k}_2 & = \mathbf{k}_3 + \mathbf{k}_4 \\ \omega_1 + \omega_2 & = \omega_3 + \omega_4 + \Delta\omega, \end{cases} \tag{2}$$

where the detuning term $\Delta\omega$ is zero for exact resonance. The resonance detuning term plays a pivotal role in the instability of the Stokes wave, which was first experimentally and theoretically discovered by Benjamin and Feir (1967). The role of the resonance detuning has been highlighted in the past decade because of its relevance in the generation of freak waves in random directional seas (e.g., Janssen 2003; Onorato et al. 2004).

A deterministic spectral evolution equation considering both the exact four-wave resonant and quasi-resonant interactions was first derived by Zakharov (Zakharov 1968):

$$i\frac{\partial b_0}{\partial t} = \omega_0 b_0 + \int T_{0123} b_1^* b_2 b_3 \delta_{0+1-2-3}\, d\mathbf{k}_{123}, \tag{3}$$

where $b_i(\mathbf{k})$ are canonical complex variables obtained by a transformation using the Fourier coefficients of the surface elevation and velocity potential in an integral power series (Krasitskii 1994). The indices $i = 0, 1, 2, 3$ are a compact notation of wavenumbers k_i, so that $T_{0123} = T(\mathbf{k}, \mathbf{k}_1, \mathbf{k}_2, \mathbf{k}_3)$ is the interaction coefficient, $\delta_{0+1-2-3} = \delta(\mathbf{k} + \mathbf{k}_1 - \mathbf{k}_2 - \mathbf{k}_3)$ is the Dirac delta function, and an asterisk represents complex conjugation. Details of the derivation of (3) and each of its terms can be found in Krasitskii (1994). Apparently, the exact resonance condition in terms of the wave frequency does not appear in (3) and, therefore, it contains exact as well as quasi-resonance interactions when $\Delta\omega/\omega_0 \sim O(\varepsilon^2)$, where ε is the representative steepness.

Equation (3) describes the evolution of a wave component through wave interaction in a four-wave combination. In the ocean, where different wavenumbers may interact in different resonant sets, a stochastic approach is more suitable. An evolution equation of the wave energy density can be readily derived from the Zakharov's equation under the quasi-Gaussian closure hypothesis (e.g., Hasselmann 1962; Yuen and Ferguson 1982; Krasitskii 1994). At a relatively long kinetic time scale $[O(\varepsilon^{-4})]$, Hasselmann's equation can be retrieved. The Hasselmann equation (Hasselmann 1962) describes the evolution of the wave action spectral density

$$\frac{\partial N_0}{\partial t} = 4\pi \int T_{0123}^2 f_{0123} \delta_{0+1-2-3} \delta(\omega_0 + \omega_1 - \omega_2 - \omega_3)\, d\mathbf{k}_{123}, \tag{4}$$

where $f_{0123} = N_2 N_3 (N_0 + N_1) - N_0 N_1 (N_2 + N_3)$. Third-generation wave forecast models do only consider exact resonance conditions, which are essential to the spectral evolution by redistributing and downshifting the input energy. However, quasi resonances, that is, $\Delta\omega \neq 0$, are also important for the evolution of statistical properties of a wave system (Annenkov and Shrira 2006), particularly in conditions of fast $O(\varepsilon^{-2})$ time-scale evolution (Gramstad and Babanin 2016). The deviation from the Gaussian statistics at this dynamical time scale is considered to be responsible for the enhanced occurrence of freak waves in the ocean, as demonstrated theoretically, numerically, and experimentally by numerous authors (e.g., Janssen 2003; Onorato et al. 2004).

The roles and interplay of exact and quasi-resonant interactions are discussed in Waseda et al. (2009b) by analyzing the evolution of random waves in a tank. The directional distribution of wave energy is tightly connected to the nature of nonlinear interactions, if driven by resonant or quasi-resonant conditions. It would then determine the primary force that controls the nonlinear interactions and the spectral evolution. It is noteworthy that in the case of a unidirectional wave field, resonant quartets do not occur, and the spectral evolution is exclusively due to quasi-resonant interactions (Waseda et al. 2009a). Quasi resonances also play a key role in the development of a spectral tail, which at dynamical time scale can be observed in the wave tank used in this study (Tanaka 2001; Waseda et al. 2009a).

A number of studies have investigated the influence of a background current on the nonlinear interactions. Qingpu (1996) derived a modified Zakharov equation that includes the effects of a shear current in the interaction coefficients. Others analyzed the modulation instability of a Stokes wave (e.g., Toffoli et al. 2013). The amplification of wave instability by adverse current gradients have been shown theoretically (Onorato et al. 2011) and experimentally (e.g., Toffoli et al. 2015; Babanin et al. 2011).

The exact resonance case under the influence of a random current field was recently studied by Waseda et al. (2015) through a series of experiments performed in the same facility as this study. By generating conditions suitable for triad interactions, where one wave component is repeated in the condition (2), they found that the energy transfer to a third originally nonexistent wave is suppressed by the background current field. The authors associated this effect with a modified wavenumber-dependent Doppler velocity due to vertical current shear

(Stewart and Joy 1974), random linear refraction due to horizontal current shear, and temporal variations of the current field. Through the numerical integration of the discretized Zakharov's equation, they have shown that a constant resonance detuning results in recurrence, whereas a randomly varying detuning suppresses the growth of the originally nonexistent wave. In other words, the short-term fluctuation of the current speed was more important than the magnitude of the mean current speed. The argument, however, is somewhat qualitative, as the relevant time scale of the current variation was not identified in their study.

The possible corollary of the aforementioned experimental result is that the background random current field will suppress the nonlinear energy transfer. To prove this hypothesis, they additionally presented a few tests for irregular directional waves, keeping the same wavemaker signal for different current conditions. The spectral tail, which is developed because of nonlinear energy cascading, is suppressed and steepens as the current speed increases.

Thus, the dynamics of nonlinear wave–current interactions is rich, and many aspects are not even known. This experiment was intended to isolate and study a selection of those. The experimental cases of the present study did not present dissipation by breaking, and the waves propagate in deep water. Therefore, it is considered that changes in the wave spectrum are caused by conservation of action due to current spatial gradients and nonlinear wave–wave interactions, which will be the two basis of our discussions. By generating a variety of initial wave conditions in a coflowing current field with similar mean velocity, we have an interesting opportunity to confirm the assumptions from Waseda et al. (2015) of current-induced detuning of four-wave interaction conditions. We further extend their analysis by investigating the impact of the random current field on different directionally distributed wave fields, from unidirectional to extremely broad spreading. Therefore, these tests provide an insight into the significance of each mechanism, that is, exact or quasi resonances, on the interaction with the currents and, particularly, how the detuning force discussed in this section impacts each case.

3. Methods

a. Facility and measurements

The Ocean Engineering Basin of the Institute of Industrial Science, University of Tokyo (Kinoshita Laboratory and Rheem Laboratory), has dimensions of 50 m × 10 m with 5-m depth. The multidirectional wavemaker is composed of 32 independent plungers, which are able to generate regular and irregular directional waves for a specified spectral shape. A current field can be generated in the wave tank both following and opposing the direction of wave propagation. The water flow is created by the circulation of the entire volume of the tank, through a water inlet and outlet located at both extremes underneath the water. A turbine moves and directs the water inside a pipe of 3 m in diameter, positioned on the side of the tank. The inlet and outlet have widths of 10 m but have different heights of 3 and 3.5 m, respectively. The generated current field is not uniform and the opposing current is considerably more unstable, with larger variation in time and space than the coflowing current, mainly due to the differences of inlet/outlet dimensions (Waseda et al. 2015). The instability increases for higher current speeds. A vertical shear is also observed (Toffoli et al. 2013). Figure 1 shows the schematic of the tank and location of wave gauges and current meters used in this experiment.

To investigate the spatial evolution of the one-dimensional spectrum, eight wave–wire gauges forming a linear array along the tank were positioned 2.5 m from the left sidewall. The first five gauges are separated by 3 m, whereas the three last gauges are 2 m apart. Besides analyzing the evolution of the one-dimensional spectrum, a geometrical configuration of six wave gauges was positioned at 32 m from the wavemaker to measure the directional spectrum. The six gauges form a pentagon with a central gauge, and the directional spectrum is obtained by using the wavelet directional method (WDM), which assumes a nonstationary wave field to determine the direction of random waves (Donelan et al. 1996). The method is based on the idea that the sea surface is represented by the superposition of wave groups propagating in different directions along the time. To compare the ability of different methods to evaluate the directional spreading of the waves in the tank, Waseda et al. (2009a) compared the WDM against the maximum likelihood method (MLM) and the maximum entropy method (MEM). Among the three methods, the WDM was the only one capable of distinguishing the different directional spreadings generated and therefore is the chosen method to be applied in the present study.

The wavemaker generates random waves with directional spreading as defined by Mitsuyasu et al. (1975):

$$G(\theta) = G_n \cos^n(\theta). \tag{5}$$

Here, we analyze the directional distribution of the generated waves based on the integral of the normalized directional distribution, as proposed by Babanin and Soloviev (1998):

$$A(f)^{-1} = \int_{-\pi}^{\pi} K(f,\theta)\, d\theta, \tag{6}$$

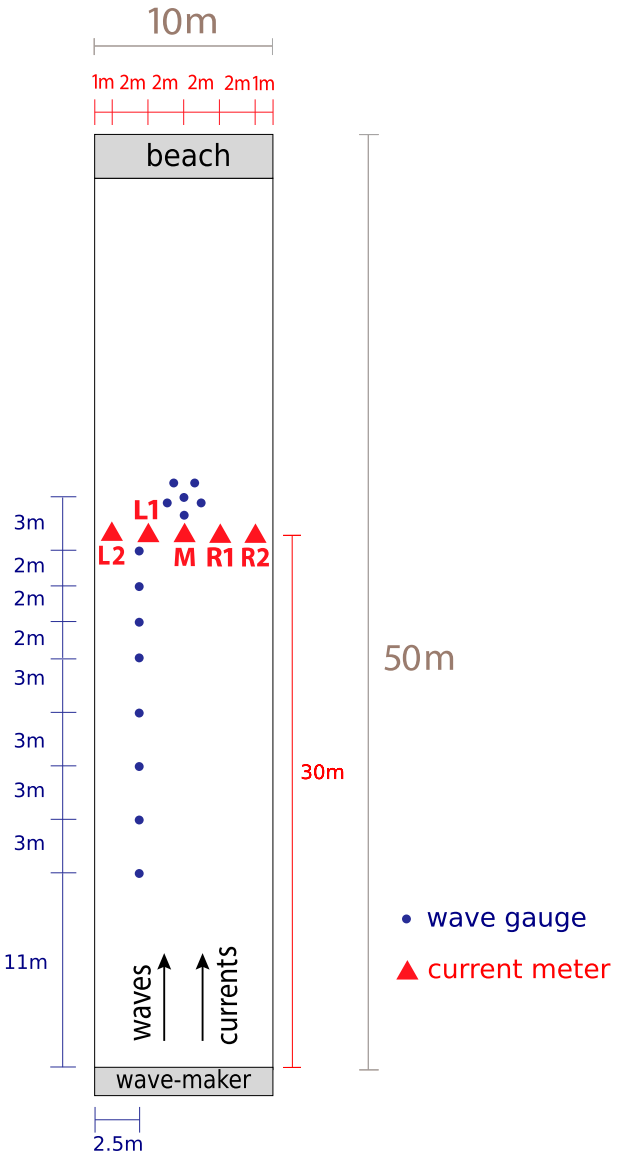

FIG. 1. Schematic of the Ocean Engineering Tank of the Institute of Industrial Sciences, University of Tokyo. Wave gauge locations are represented by blue circles, and current meters are represented by red triangles.

where $K(f, \theta)$ is the directional distribution normalized with respect to the maximum value in the dominant direction $\theta_{\max}$, so that $K(f, \theta_{\max}) = 1$ and $G(f, \theta) = AK(f, \theta)$. The parameter A represents the inverse normalized directional spectral width. It is related to the parameter n, of $\cos^n$ spreading forms, by

$$A = \frac{\Gamma(n/2 + 1)}{\pi^{1/2}\Gamma(n/2 + 1/2)}, \tag{7}$$

where Γ is the gamma function. The convenience of using the parameter A to represent the directional spreading is that the integration of the normalized directional distribution avoids uncertainties in the directional width resultant from irregularities of a measured spectrum. Moreover, Babanin and Soloviev (1998) provide its relation to other existing and widely used spreading forms. Hereinafter, parameter A refers to the value of the inverse normalized directional distribution at the peak frequency, that is, $A(f_p)$. Therefore, higher values of A correspond to narrower directional distribution of wave energy at the peak frequency.

b. *Characteristics of the current field*

Prior to the wave experiments, a current field was generated in the tank with magnitude set to 7.5 cm s^{-1} toward the end of the tank (beach), which was the chosen current to be generated for all the wave cases analyzed in this study. To confirm the nonhomogeneity of the current observed in previous experiments (e.g., Toffoli et al. 2013; Waseda et al. 2015), an electromagnetic current meter was positioned at 30 m from the wavemaker in five different locations, 2 m apart (red triangles in Fig. 1). Although the five measurements were not performed simultaneously, the results provide a sense of the cross-section profile of the current field. Speed and direction for the five locations are shown in Fig. 2. R2 and L2 are positions at the most extreme right and left sides, respectively, relative to the direction of wave propagation. Mean value μ and standard deviation (std dev) at each point are shown in Table 1.

The most noticeable feature observed from Fig. 2 is the significantly higher standard deviation (in Table 1) of the current speed at the right-hand side of the tank (position R2). The variability of the current reaches values of 40% of the mean speed at position R1. Conversely, the left side (points L1 and L2) shows mean speed of more than 2 cm s^{-1} slower than at R2 and a comparatively steady flow. The directional variation follows the same patterns as the current magnitude; with overall deviation to positive values (0° is longitudinal). Therefore, the intensity and direction of horizontal shear is modified along the time. A similar behavior of the currents in the tank was observed by Waseda et al. (2015) for opposing currents. Simultaneous measurements performed by Toffoli et al. (2013) also show that the spatial and temporal variability of the flow is substantial.

A Lagrangian approach to estimate the spatial distribution of the current field in the tank was applied by Takahashi (2011) using particle tacking velocimetry (PTV) methods. The floating drifters converged on the left side, indicating slower velocities on this side, as also shown in our analysis. Although the analyzed domain

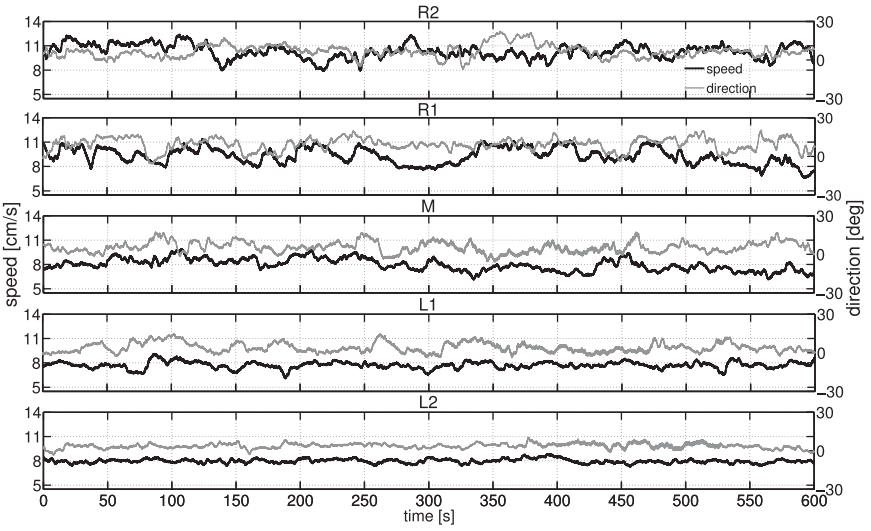

FIG. 2. Time series of current speed (thick black line) and direction (gray line) at the five locations in a cross section at 30 m from the wavemaker, where R2 and L2 are the most right and left points, respectively (from the wavemaker point of view). Positions are shown in Fig. 1 by the red triangles.

covers only a rectangular section of the tank, the most relevant result is that the current distribution is highly variable in both the cross- and along-channel directions.

A more unsteady flow is associated with stronger shear. The fluctuations of velocity and direction on the right-hand side (positions R1 and R2) can be used to estimate the main eddy scales in the tank. We can observe different fluctuations with specific time scales. Considering fluctuations greater than 10% with respect to the mean velocity, we identify a few longer fluctuations at position R1 (highest std dev) of approximately 30 s with a fluctuating velocity of $\sim 2\,\mathrm{cm\,s^{-1}}$. If we consider the advective velocity as $u_{\mathrm{ad}} = \overline{u} + u'$, where $\overline{u}$ and u' are the mean and fluctuating components, respectively, the length scale of these larger eddies would be of ~ 3 m. However, the most common and defined fluctuations observed are of 7–10 s, with fluctuating velocities in the range 1–1.5 $\mathrm{cm\,s^{-1}}$, which would be associated with length scales of 0.8–1.1 m. Other well-defined fluctuations would be related to ~0.4-m length scales. Therefore, the scales of the main eddies, where the flow is more turbulent, range from tens of centimeters to a few meters, with a progressive weakening toward the left side of the channel. The current on the left side will thus produce less intense wave refraction, while the direction of wave propagation on the right-hand side is expected to be deviated more sharply.

For all the experimental cases, the generated current follows the direction of wave propagation (positive sign). The electromagnetic current meter was positioned in the middle of the tank at 30 m from the wavemaker (position M in Fig. 1). Thus, it was not possible to measure the transversal current gradient for all experiments. Based on our observations and on the results in Takahashi (2011), Toffoli et al. (2013), and Waseda et al. (2015), we consider the current field as randomly variable, which hinders a precise modeling of wave propagation.

c. *Experimental setup*

The analysis of four groups of experiments are presented, in each of which the same initial wave conditions are generated in the absence and presence of a coflowing current field. In the first group, we test the propagation of an initial single monochromatic wave train characterized by period T and steepness ak (where a is the wave amplitude and k is the wavenumber). The second set of experiments was performed for initial, unidirectional random waves based on the Joint North Sea Wave Atmosphere Project (JONSWAP) spectral formulation (Hasselmann et al. 1973) with varying steepness. The third and fourth groups are represented by

TABLE 1. Statistics of current speed U and direction θ_U of the plots of Fig. 2; μ is the mean value and std dev indicates the standard deviation. Positions are shown in Fig. 1 by the red triangles.

Position	$\mu(U)$ ($\mathrm{cm\,s^{-1}}$)	Std dev (U) ($\mathrm{cm\,s^{-1}}$)	$\mu(\theta_U)$ (°)	Std dev (θ_U) (°)
R2	10.31	0.86	6.76	4.78
R1	9.30	1.00	9.42	4.89
M	7.94	0.74	5.52	4.22
L1	7.73	0.41	4.01	3.72
L2	7.97	0.25	3.71	1.90

TABLE 2. Details of experiments performed. The terms Mono, JON-1D, and JON-2D refer to regular monochromatic, unidirectional, and directional waves based on the JONSWAP spectral formulation, respectively.

Group	Case	Type	f_p (Hz)	k_p (rad m^{-1})	kh	α	γ	ε	A
1	1	Mono	1.11	4.96	24.79	—	—	0.05	—
	2	Mono	1.11	4.96	24.79	—	—	0.08	—
2	3	JON-1D	1.25	6.28	31.44	0.0063	1	0.05	—
	4	JON-1D	1.25	6.28	31.44	0.0063	5.5	0.07	—
	5	JON-1D	1.25	6.28	31.44	0.0063	17	0.10	—
3	6	JON-2D	1.25	6.28	31.44	0.0041	3.3	0.05	2
	7	JON-2D	1.25	6.28	31.44	0.0080	3.3	0.07	2
	8	JON-2D	1.25	6.28	31.44	0.0164	3.3	0.10	2
4	9	JON-2D	1.25	6.28	31.44	0.0194	5.0	0.12	1.5
	10	JON-2D	1.25	6.28	31.44	0.0194	5.0	0.12	2.5
	11	JON-2D	1.25	6.28	31.44	0.0194	5.0	0.12	3.5

directional random waves, first varying the steepness for the same directional spreading and, finally, varying the directional distribution for a similar 1D spectral form. For the random cases, the wave steepness is defined as $\varepsilon = ak_p$, where $a = \sqrt{2}\sqrt{m_0}$ is the mean amplitude (in which m_0 is the total variance or integrated spectral energy) and k_p is the wavelength at the spectral peak. Table 2 shows the list of experiments performed. All the irregular wave cases were recorded for 15 min, whereas the regular waves were for 10 min.

The experiments were planned in order to generate a broad range of initial wave conditions. The two main wave characteristics we judge to be fundamental in this study are the wave steepness and the directional distribution. Therefore, the experiments aim to vary one of these two parameters within the respective groups. As a consequence, nonlinear wave–wave interactions are expected to increase between the cases of each group. Waseda et al. (2015) briefly investigated the effect of adverse currents on the same wave field and their impact on quasi-resonant interaction. They observed the steepening of the high-frequency spectral tail (f in the range 1.56–3.03 Hz) as the current speed increases. Here, we add different types of initial conditions for random waves with varying wave steepness and directional spreading on coflowing currents. By doing so, the nonlinear interactions potentially intensify within the groups, and a similar background current field is expected to affect each case differently. It should be noted that no breaking was observed, eliminating any dissipation concerns.

Table 3 compares the aimed to the measured values of the main wave parameters and mean current speed $\overline{U}$. The wave measurement corresponds to the mean value among the gauges in the pentagon. The relation $\overline{U}/c_g$ is also shown. Although there are differences between aimed and measured values, the main goal of the experiments were achieved, that is, to generate cases with considerable differences in wave steepness (first three groups) and keep a similar steepness with varying directional spreading (last group).

4. Results and discussion

Our interest is in the transformation of the wave spectrum by comparing the same generated wave field (signal sent to wavemaker) in the absence and presence

TABLE 3. Aimed P and measured P^* parameters of the experiments performed.

Group	Case	$T_p(s)$	$T_p^*(s)$	ε	ε^*	A	A^*	$\overline{U}$ (cm s^{-1})	$\overline{U}^*$ (cm s^{-1})	$\overline{U}^*/c_g$
1	1	0.9	0.89	0.05	0.051	—	21.9	7.5	6.68	0.097
	2	0.9	0.89	0.08	0.077	—	33.8	7.5	7.17	0.103
2	3	0.8	0.88	0.05	0.056	—	7.9	7.5	7.28	0.106
	4	0.8	0.85	0.07	0.073	—	11.4	7.5	6.90	0.104
	5	0.8	0.89	0.10	0.090	—	11.3	7.5	7.08	0.102
3	6	0.8	0.85	0.05	0.044	2.0	2.26	7.5	7.54	0.121
	7	0.8	0.85	0.07	0.070	2.0	3.08	7.5	7.57	0.122
	8	0.8	0.87	0.10	0.106	2.0	2.32	7.5	7.33	0.108
4	9	0.8	0.84	0.12	0.121	1.5	1.3	7.5	7.17	0.111
	10	0.8	0.91	0.12	0.110	2.5	2.1	7.5	7.30	0.103
	11	0.8	0.92	0.12	0.119	3.5	4.0	7.5	7.26	0.098

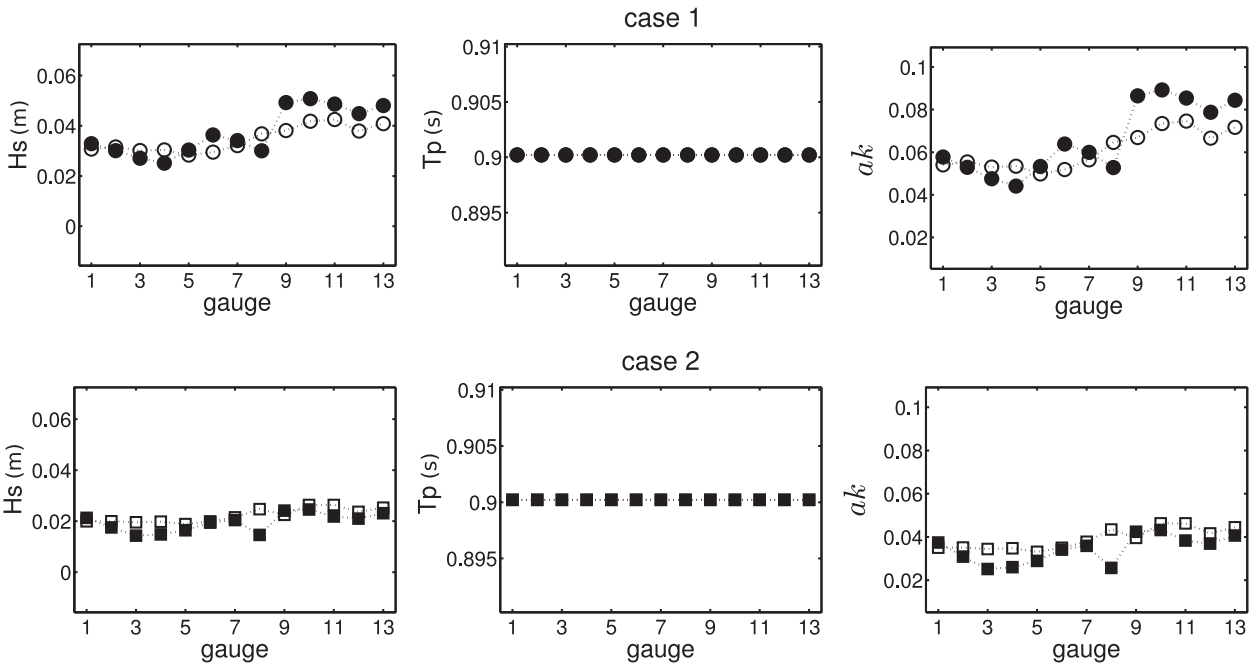

FIG. 3. Measured wave parameters of significant wave height H_s, peak period T_p, and steepness ak (from left to right, respectively) in the presence (filled markers) and absence (open markers) of currents for the two monochromatic cases: 1 (circles) and 2 (squares). The first eight gauges are from the linear array on the left side of the tank, while the last five compose the pentagon array in the middle of the tank (at 32 m from the wavemaker).

of currents. For the monochromatic cases, our analysis is also focused on the wave parameters, such as wave height and period, which provides a sense of the current distribution in the tank. For irregular waves, we turn our attentions mainly to the high-frequency part of the spectrum and directional distribution of energy.

The wavemaker frequency upper limit is 2.5 Hz; however, it has been shown that, despite the short time scale of tank experiments, the nonlinear energy transfer to higher frequencies occurs at such a fast rate (Tanaka 2001) that a tail beyond this limit is developed by dynamical cascading (Waseda et al. 2009a). Therefore, the spectral energy observed above 2.5 Hz is purely originated from four-wave interactions [(3)], and hence the wave components must meet the quadrilateral condition (2). This process gives us the opportunity to investigate how the random current field would perturb the nonlinear interactions and the development of the spectral tail, according to the discussion in the end of section 2. Transformations of the directional spectrum of irregular waves caused by the current field are shown and the results are discussed.

a. Group 1: Regular waves

The first group of experiments is represented by single wave trains with $T = 0.9$ s and varying steepness. The measured wave parameters of significant wave height H_s, spectral peak period T_p, and steepness ak are shown in Fig. 3. The H_s exhibits little variation along the tank when currents are absent; T_p shows no change when in the presence of currents and no variation along the tank. According to the linear theory, current-induced changes in the absolute frequency ω are related to the temporal variability of the current $\partial U/\partial t$ (see section 2), which indicates that the current at these points is not effectively unsteady.

The two wave trains exhibit different patterns when in the presence of currents. Both have their wave energy decreased at most gauges of the linear array (eight initial points). However, at the pentagon gauges (last five points), the first case ($ak = 0.08$) shows an increase, while the second ($ak = 0.05$) shows a decrease of energy. These patterns are probably being controlled by refraction-induced convergence or divergence of wave energy, and it varies among the cases due to temporal variations in the spatial distribution of the current field (see Fig. 2 and the discussion in the appendix). Variations in steepness follow variations in H_s. The time series of surface elevation indicate that the energy varies considerably in all wave sensors along the time, with no clear pattern.

An alternating pattern of refractions can be seen by means of the directional spectrum (Fig. 4). To show variations along the time, the measured time series were

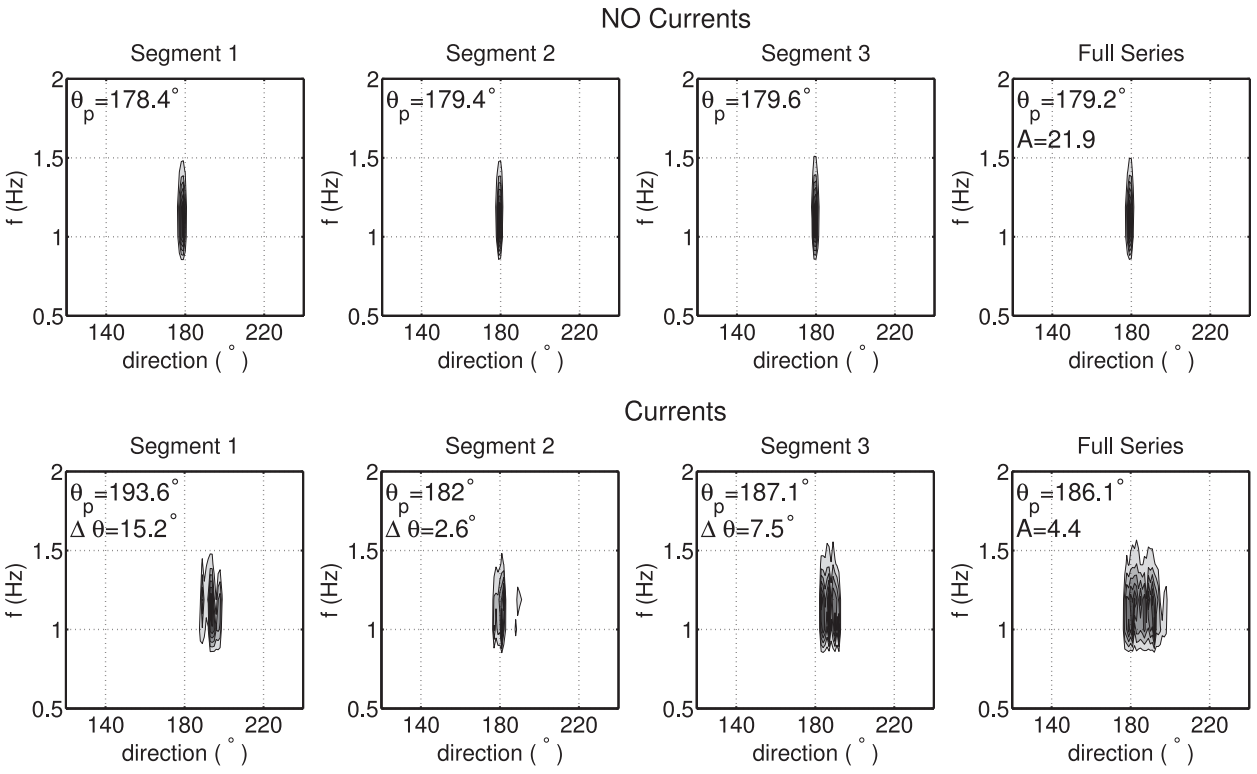

FIG. 4. Directional spectra obtained for the monochromatic case 1 in the (top) absence and (bottom) presence of currents. The elevation time series were divided in three segments. Plots from left to right show each segment and full time series spectra. Peak direction θ_p, the difference of θ_p in the absence and presence of currents ($\Delta\theta_p$), and A obtained for the full series are shown.

divided in three segments. Figure 4 shows the example of case 1. By obtaining the directional spectrum of each segment, it is possible to see that the current-induced refraction is not constant along the recorded time but exhibits random variations. The bottom panels show the directional shift of the spectral peak $\Delta\theta$. This unpredictable behavior creates zones of convergence or divergence of energy in the tank as well as consecutive disturbances in wavenumbers. The spectra are apparently broadened and the final spectrum is highly perturbed.

If we invoke "frozen turbulence," assuming that the mean current speed observed at the two sides of the tank (R2 and L2; see Table 1) generates a homogeneous cross-channel gradient along the tank, we can apply the geometrical optics approximation to infer refractions undertaken by the wave rays. Refractions of a regular wave of $T = 0.9$ s ($L = 1.26$ m) would be of 3.5° at the point where the directional spectrum is obtained. However, the random fluctuations in current speed and direction generate a highly variable current field. By dividing the time series of surface elevation and obtaining the directional spectrum of a regular wave (Fig. 4), we observe that the wave direction randomly varies along the time, with $\Delta\theta$ from 2.6° to 15.2°. This supports the assumption of a variable and unsteady current field, which is associated with sharp gradients.

The mean current speed values (Table 1) suggest a nonhomogeneous cross-section gradient, which would consequently create zones of convergence and divergence of wave energy. The results of Takahashi (2011), applying a PTV method, showed that the current velocity in the along-tank direction is also considerably variable. Furthermore, the right-hand side of the tank exhibits a significantly higher standard deviation of current speed and direction, which would contribute to the random character of the refraction process. Current-induced focusing and defocusing of wave energy are likely to be responsible for the changes in the wave height observed in Fig. 3 (see the appendix for a discussion on wave refraction and energy focusing in the tank).

From the analysis of single wave trains, we can conclude that the current field is highly variable in its spatial distribution. Although temporal variations exist, they were not effective in changing the absolute wave period. However, wavenumber and direction are randomly modified. Our results indicate that energy focusing/defocusing that originated from the alternating refraction

patterns is the cause of wave height variations. The task of representing a good approximation of the current field for modeling purposes is thus complicated with many uncertainties involved.

b. Irregular waves

From the first group of experiments, it was possible to have a more thorough understanding of the current field and its effects on single wave trains. Groups 2, 3, and 4 are represented by irregular wave fields based on the JONSWAP spectral formulation, which assumes an equilibrium tail proportional to f^{-5}:

$$E(f) = \alpha g^2 (2\pi)^{-4} f^{-5} \exp\left[\frac{-5}{4}(f/f_p)^{-4}\right] \gamma^{\exp[(f-f_p)^2/(2\sigma^2 f_p^2)]}, \tag{8}$$

where $\sigma = 0.08$, f_p is the peak frequency (which is set to ~1.25 Hz for all cases), α controls the energy level, and γ affects the spectral peakedness. The steepness can be manipulated by varying both α and γ. The latter, however, has direct implications on the frequency bandwidth and consequently on the instability of nonlinear groups (Ribal et al. 2013) by strengthening the quasi-resonant interactions. The peakedness γ assumes values of 1, 5.5, and 17 for the unidirectional waves (group 2), whereas α is the chosen parameter that controls the steepness of directional waves (group 3), assuming values of 0.0041, 0.0080, and 0.0164. Thus, our attentions are on steepness variations via changing one of both, γ or α, while the other is retained. In the last group of experiments (group 4), we investigate different directional spectral width (A = 1.5, 2.5, and 3.5) for a similar directionally integrated spectrum.

c. Spectral downshifting

The distribution of wave parameters along the tank follows similar patterns to the regular waves, except for peak period T_p. In the presence of currents, the integrated spectral energy, represented by parameter H_s, is always decreased at the linear array (left-hand side of the tank), whereas the pentagon of gauges show at times increasing and at times decreasing of energy (not shown here). This supports the assumption of a randomly variable current field with different time scales of temporal variation.

A progressive downshifting of the spectral peak along the fetch is observed in the absence of currents, which, since energetic breaking is absent, is associated with nonlinear interactions (Waseda et al. 2009b). In the presence of currents, the downshifting can also be observed; however, it is slower or less intense. To quantify the downshifting, we calculate the ratio between the average peak frequency between 10 and 17 m (ω_i; first three gauges) and at 32 m (ω_f; pentagon of gauges). The relations of the ratio ω_i/ω_f with steepness ε and the directional parameter A are shown in Fig. 5 for all the irregular wave cases (groups 2–4 in Table 2).

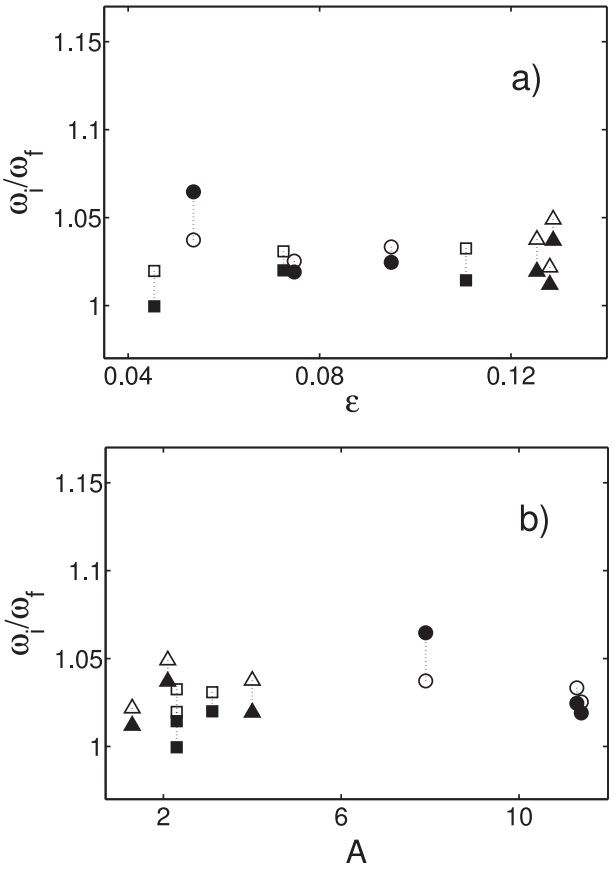

FIG. 5. Relation between frequency downshift and (a) steepness ε and (b) parameter A for irregular wave cases: varying γ (circles, group 2), varying α (squares, group 3), and varying directional parameter A (triangles, group 4). Open symbols show cases in the absence of currents. Filled symbols indicate the presence of currents. Downshift is quantified as ω_i/ω_f, where ω_i is average peak frequency between 10 and 17 m and ω_f at 32 m.

When currents are absent, the downshifting ratio is within 5%, which agrees with the experimental results of Waseda et al. (2009b) for a similar fetch range and peak wavelength. It seems that there is no clear dependence on the initial steepness or directional width. In the presence of currents, the rate of spectral downshifting decreases for all cases, except one. This case is represented by the first case of the varying γ group, having the lowest steepness and broadest frequency bandwidth within the group. For this case, the spectra showed an almost "flat" or slightly bimodal shape (see Fig. 7 upper-left panel), the identification of the spectral peak was inaccurate, and no progressive downshifting was seen

along the fetch. Because in the absence of breaking the downshifting is connected to both exact and near-resonant interactions, we conjecture that the presence of a background current field perturbs the conditions of four-wave interactions [(2)], as suggested by Waseda et al. (2015). Consequently, the rate of peak downshifting is slowed. The process of current-induced detuning and its consequences on the high-frequency part of the spectrum will be discussed in detail in the following sections.

1) GROUPS 2 AND 3: VARYING STEEPNESS CASES

The comparison of the spectra in the absence of currents for groups 2 and 3 is shown in Fig. 6 (top and bottom panels, respectively). As expected, the steepness ($\varepsilon = ak_p$) increases considerably as γ and α assume greater values. The initial JONSWAP form imposes an energy decay at a rate proportional to f^{-5}, up to around 2.5 Hz. However, the spectra within each group show different characteristics in the high-frequency region, above the wavemaker upper limit of 2.5 Hz (vertical dashed line). This limit is clearly marked for some cases and is associated with a sudden steepening of the spectral tail. Remarkably, the sudden drop of the tail is more prominent for the lowest ε cases, and it is almost imperceptible for the highest ε spectra. A spectral tail is developed beyond 2.5 Hz by wave–wave interactions (Waseda et al. 2009a). From Fig. 6, we see that the development is stronger for the steeper spectra and the tail approximates the f^{-5} decay. Therefore, the tail developed beyond the generated frequencies will be used as an indicator of the strength of nonlinear interactions and energy cascading.

By adding a background current field, the wave spectrum undertakes considerable changes (Fig. 7). The energy decreases around the peak probably due to the divergence effects on the left-hand side of the tank (see Fig. 3). These changes are somehow random and not clearly patterned. However, the high-frequency tail (i.e., for $f > 2.5$ Hz) exhibits an interesting pattern when in the presence of currents. The tail is suppressed and steepened. The tail differences between corresponding spectra in absence and presence of currents are greater for the steeper cases. The larger the spectral steepness ε, the more intense the nonlinear interactions and energy cascading. As a consequence, the current-induced perturbations of the tail are more evident.

Our results corroborate the arguments of Waseda et al. (2015) of current-induced detuning of the conditions of four-wave interactions. The detuning would be a result of the Doppler shift and random refraction. The cumulative effect of a wavenumber-dependent Doppler velocity caused by current vertical shear (Toffoli et al. 2013) would be significant for the detuning term $\Delta\omega$ in

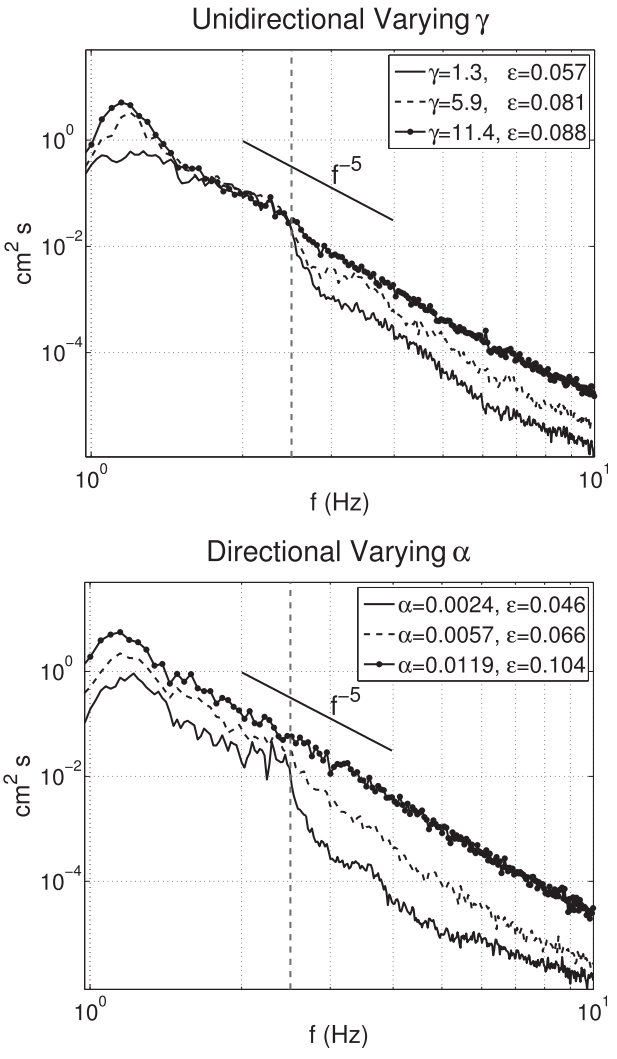

FIG. 6. Frequency spectrum for (top) unidirectional and (bottom) directional random waves in the absence of currents. Measurements are from gauge 4 at 20 m from the wavemaker. Theoretical f^{-5} decay is shown (solid black line). The spectra were estimated using average periodograms with 50% overlap, Hanning window, and frequency resolution of 0.0244. Vertical dashed line draws the wavemaker upper limit.

(2), since $\Delta_{kU} = \mathbf{k}_1 \cdot \mathbf{U}_1 + \mathbf{k}_2 \cdot \mathbf{U}_2 - \mathbf{k}_3 \cdot \mathbf{U}_3 - \mathbf{k}_4 \cdot \mathbf{U}_4 \neq 0$. Additionally, random refraction will perturb the resonance condition of wavenumber

$$\mathbf{k}_1 + \mathbf{k}_2 - \mathbf{k}_3 - \mathbf{k}_4\big|_{t=t_1} = \int_{t_0}^{t_1} \Delta\nabla_{kU}\, dt. \qquad (9)$$

The authors support their hypothesis by numerically simulating the Zakharov equation (3) for the exact resonance case with the addition of a detuning term to represent $\Delta\omega$ in (2). As the randomly varying detuning increases, the growth of the originally nonexisting wave

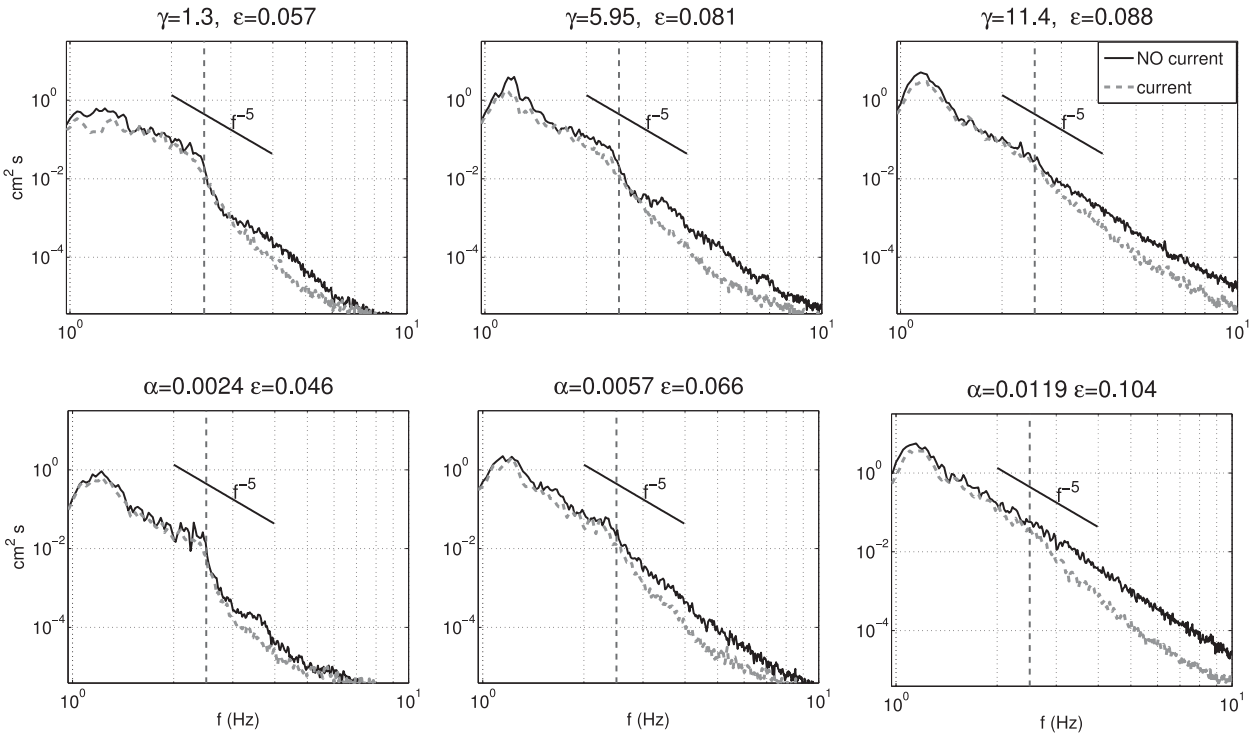

FIG. 7. Frequency spectrum at gauge 4 for (top) all unidirectional, varying gamma and (bottom) directional, varying alpha cases. Solid black line shows spectrum with no current and dashed gray line shows spectrum in the presence of currents. Theoretical f^{-5} decay is shown. Vertical dashed line draws the wavemaker upper limit. Spectral estimation method applied is the same as described in Fig. 6.

slows and eventually saturates. They found the results in agreement with the experimental simulation of a same quartet. Therefore, the experimental and numerical results of Waseda et al. (2015) support the hypothesis that the random current field annuls the resonant conditions, with the consequent suppression of the spectral tail.

2) GROUP 4: VARYING DIRECTIONAL SPREADING CASES

The last group of experiments is represented by initial spectra with similar directionally integrated form, represented by $f_p = 0.8$ Hz, $\gamma = 5.0$, and $\alpha = 0.194$, but varying directional spreading ($A = 1.3, 2.1$, and 4.0). The cases of $A = 1.3$, 2.1, and 4.0 correspond to $n = 10$, 32, and 100 of the Mitsuyasu directional spreading function $G(\theta) = G_n \cos^n\theta$, respectively. We chose a reasonably high value for steepness ($\varepsilon = 0.12$) in order to activate the nonlinear interactions but not high enough to produce energetic breaking. In directionally confined wave fields, the evolution of the spectrum is primarily controlled by quasi-resonant interactions. When the spectrum is considerably broad, exact resonances are the principal mechanism of energy exchanges. Therefore, this group of experiments aims to investigate the effect of the current field on the interplay between quasi-resonant and resonant interactions.

The measured spectra in the absence of currents are shown in the left panel of Fig. 8. As intended, the 1D spectral geometry are remarkably similar, and little difference can be noticed. Diverging from the previous groups, the wavemaker limit is not distinguishable, and all the spectra develop a high-frequency tail that approximates an f^{-5} decay above 2.5 Hz. The values of H_s obtained were 0.064, 0.070, and 0.070 m for the cases $A = 1.3$, 2.1, and 4.0, respectively. A small difference in peak frequency was observed, with measured values of 1.20, 1.15, and 1.17 Hz, respectively.

Comparisons with the corresponding spectra in the presence of coflowing currents are shown in the right-hand side panels of Fig. 8. In the absence of currents, the equilibrium tail in the frequency range $1.35f_p$–$2f_p$ (indicated in the plots) shows a higher stage of development as the directional spreading broadens. The values of the exponent ν of the tail decay $f^{-\nu}$ obtained for the equilibrium range were of 3.9, 4.62, and 5.05 for $A = 1.3$, 2.1, and 4.0, respectively. This result agrees with Waseda et al. (2009b), where a larger number of initial directional distributions were tested for the same JONSWAP spectral shape. It is worth noting that a decay rate to the power of −4 is representative of resonant interactions. As the energy is distributed in a sufficiently broad range of directions, exact resonances control the

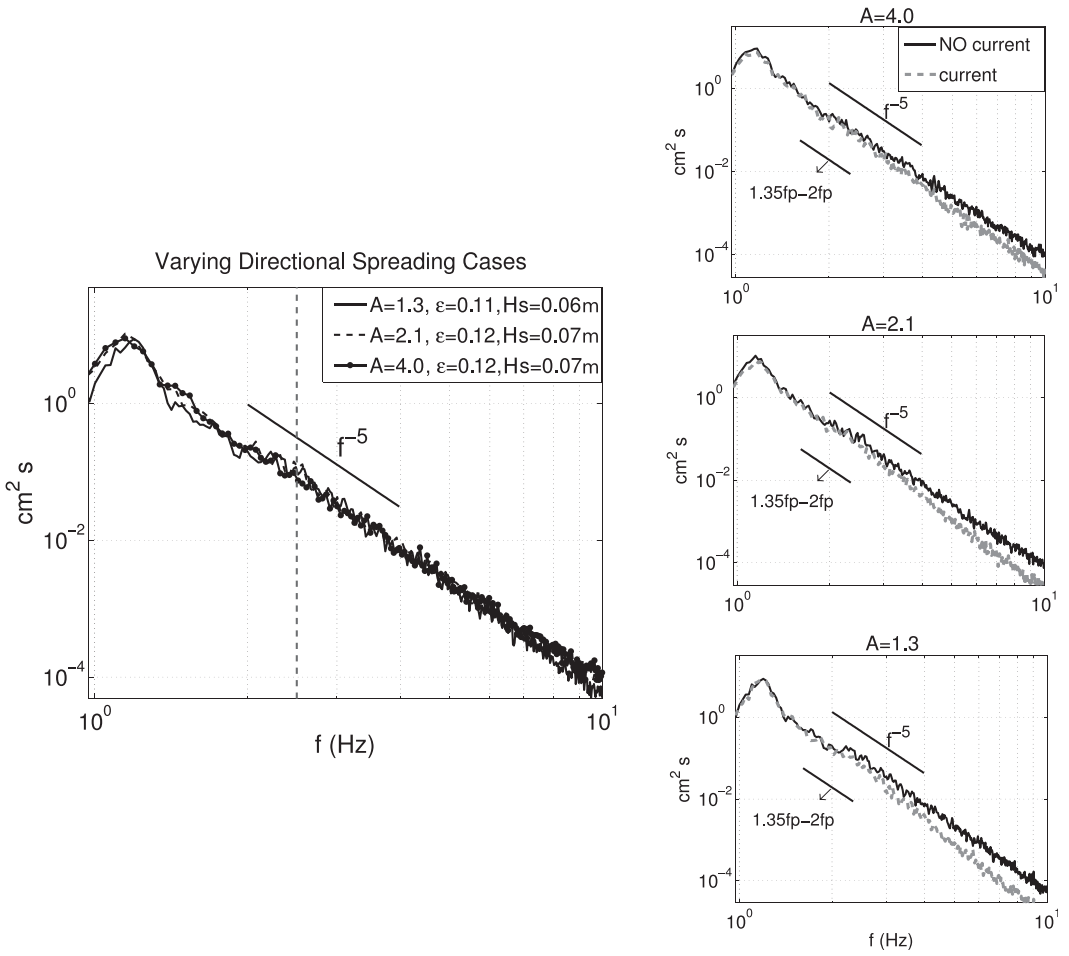

FIG. 8. Frequency spectrum for directional random waves with varying directional spreading ($A = 1.5$, 2.5, and 3) in the (left) absence and the (right) comparison of absence and presence of currents. Measurements are from gauge 3 at 17 m from the wavemaker. Theoretical f^{-5} decay is shown for all plots and line representing decay at the frequency range ($1.35f_p$–$2f_p$) is shown in the right panels. Vertical dashed line draws the wavemaker upper limit. The spectra were estimated using average periodograms with 50% overlap, Hanning window, and frequency resolution of 0.0244.

evolution of the spectral form and are associated with the downshifting of the spectral peak as well as the maintenance of the equilibrium tail (Waseda et al. 2009b). This explains the slower decay in the equilibrium range for the broadest case. However, beyond 2.5 Hz the energy decay is highly similar for the three cases ($A = 1.3$, 2.1, and 4.0), with $\nu = 5.40$, 6.00, and 5.44, respectively, which are similar to the highest steepness cases of groups 2 and 3.

To have a better understanding of the relative significance of the mechanism at work (resonances or quasi resonances) in the three cases, we calculate the kurtosis as a function of the Benjamin–Feir index (BFI) and the directional spreading, as proposed by Mori et al. (2011). The kurtosis μ_4 is related to the wave grouping and quasi-resonant interactions in an unidirectional wave field based on the ratio of the steepness to frequency bandwidth. It was extended by Mori et al. (2011) to include the directionality of the wave field using a directional or effective Benjamin–Feir index (BFI_{2D}):

$$\mu_4 = 3 + \frac{\pi}{\sqrt{3}}\mathrm{BFI}_{2D}^2, \tag{10}$$

where

$$\mathrm{BFI}_{2D}^2 = \frac{\mathrm{BFI}^2}{1 + cR}, \tag{11}$$

in which $\mathrm{BFI} = (\sqrt{2}\sqrt{m_0}k_p)/\delta_\omega$ is the BFI for unidirectional waves, δ_ω is the frequency bandwidth, $R = (1/2)\delta_\theta^2/\delta_\omega^2$ is an effective bandwidth, and c is an empirical coefficient found to be $c = 7.1$. For obtaining a representative δ_ω, all the wave gauges in the pentagon are considered. The kurtosis, parameterized by the BFI_{2D} (Mori et al. 2011), has been shown to monotonically

increase as the directional spreading narrows, with values of 3.02, 3.06, and 3.2 for $A = 1.3$, 2.1, and 4.0, respectively. Therefore, the role of the quasi resonances becomes more important as the directional spreading narrows. Furthermore, Waseda et al. (2009a) analyzed the relation of kurtosis and the spreading parameter A and suggested that a value of $A = 4.0$ is the transition from the predominance of exact resonances to quasi resonances in the nonlinear energy transfer, which reinforces the suggestion that in the last case ($A = 4.0$) quasi resonances are the primary mechanism at work.

When the currents are present, the high-frequency energy is suppressed. This effect, which was evident for the high ε cases of groups 2 and 3, is more prominent as the directional spreading broadens. This suggests that the detuning of nonlinear interaction conditions caused by the random currents is more efficient when exact resonances are dominant. As the spectrum narrows in direction, quasi resonances are in turn the primary mechanism of interactions. The tail is also suppressed, however, not as intensely, which indicates that the detuning force is less effective.

The impact of currents on the different spectra is better visualized by looking to the evolution of individual cases along the fetch. Figure 9 shows the spatial evolution of the wave spectrum for the directionally broadest ($A = 1.3$) and narrowest ($A = 4.0$) cases (Figs. 9a and 9b, respectively). The 1D spectra at the eight wave gauges of the linear array are plotted. Spectra with and without currents are compared (Figs. $9a_1$ and $9b_1$). To quantify the suppression of the high-frequency energy, we calculate the integral of the normalized difference in the high-frequency spectral energy in the absence E and presence E_c of currents, that is,

$$\Delta\overline{E}_{\mathrm{hf}} = \frac{1}{f_2 - f_1}\int_{f_1}^{f_2} \frac{E(f) - E_c(f)}{E(f)}\,df. \tag{12}$$

Here, the frequency limits applied were $f_1 = 2$ Hz and $f_2 = 7$ Hz, hence emphasizing the energy generated exclusively by nonlinear interactions. The random detuning force tends to weaken for both cases as the waves propagate along the fetch and to eventually reach a saturation stage. The evolution of $\Delta\overline{E}_{\mathrm{hf}}$ (Figs. $9a_2$ and $9b_2$) decreases along the fetch, however, in different manners. In directionally broad initial waves (Fig. 9a), the current-induced suppression of the high-frequency energy is evident. The detuning force (represented by $\Delta\overline{E}_{\mathrm{hf}}$) persists and reaches its maximum at ~14 m, decreasing as waves approach the last three wave gauges (25–29 m). For the narrowest initial wave field ($A = 4.0$), the difference between the spectra in the absence and presence of currents is practically only noticed at the first three gauges. The $\Delta\overline{E}_{\mathrm{hf}}$ rapidly decreases to null or even negative values. Figures $9a_3$ and $9b_3$ show the evolution of the decay exponent ν of the high-frequency tail $f^{-\nu}$. The tail of the spectra, both in the presence and absence of currents, tends to steepen between the 11- and 25-m gauges with very similar patterns regardless of the presence of background currents. These results reinforce the suggestion that the current-induced detuning of nonlinear interactions is more effective for spectra in which exact resonances prevail. When quasi resonances are dominant, the suppression of high-frequency energy is less prominent and short lived along the fetch.

From the results for irregular waves, it is observed that as the steepness increases, the spectral tail is more developed and consequently more affected and suppressed by the random current. Moreover, it seems that the resonance detuning is more effective as the distribution broadens (lower values of A). To expresses the effectiveness of the detuning force, we introduce a straightforward parameter that weights the steepness ε with the directional spreading parameter A:

$$\varepsilon_A = \frac{\varepsilon}{A}. \tag{13}$$

Figure 10 shows the evolution of the decay exponent ν of the tail $f^{-\nu}$ as a function of steepness (Fig. 10a) and parameter A (Fig. 10b) for all irregular wave cases (i.e., cases 3–11). Figures 10d and 10e show $\Delta\overline{E}_{\mathrm{hf}}$ as a function of ε and A, respectively. The results show the mean value among gauges 2–5, at which the effects of currents were seen to be more evident. The tail decay exponent ν was obtained from the frequency interval 2–4 Hz.

Results of Fig. 10a demonstrate that the development of the tail is tightly related to the increase of steepness, and it reaches a saturation stage close to $f^{-\nu}$. The relation of ν with ε seems to not distinguish between unidirectional (group 2) and directional (groups 3 and 4) wave fields. In Fig. 10d (ε vs $\Delta\overline{E}_{\mathrm{hf}}$), we can see the impact of the current on this process. For steeper waves, parameter $\Delta\overline{E}_{\mathrm{hf}}$, which quantifies the suppression of the tail energy, reaches larger values.

By analyzing the relations of ν and $\Delta\overline{E}_{\mathrm{hf}}$ with the directional parameter A (middle column plots of Fig. 10), an interesting characteristic is seen. There seems to be no direct dependence of the high-frequency tail exponent ν on parameter A (Fig. 10b); however, the energy difference at high frequencies $\Delta\overline{E}_{\mathrm{hf}}$ is always small for directionally confined wave fields (Fig. 10e). For small values of A (broad waves), $\Delta\overline{E}_{\mathrm{hf}}$ is highly variable and it depends on the spectral steepness. This evidence suggests that when quasi-resonant interactions are predominant, the detuning force caused by currents is

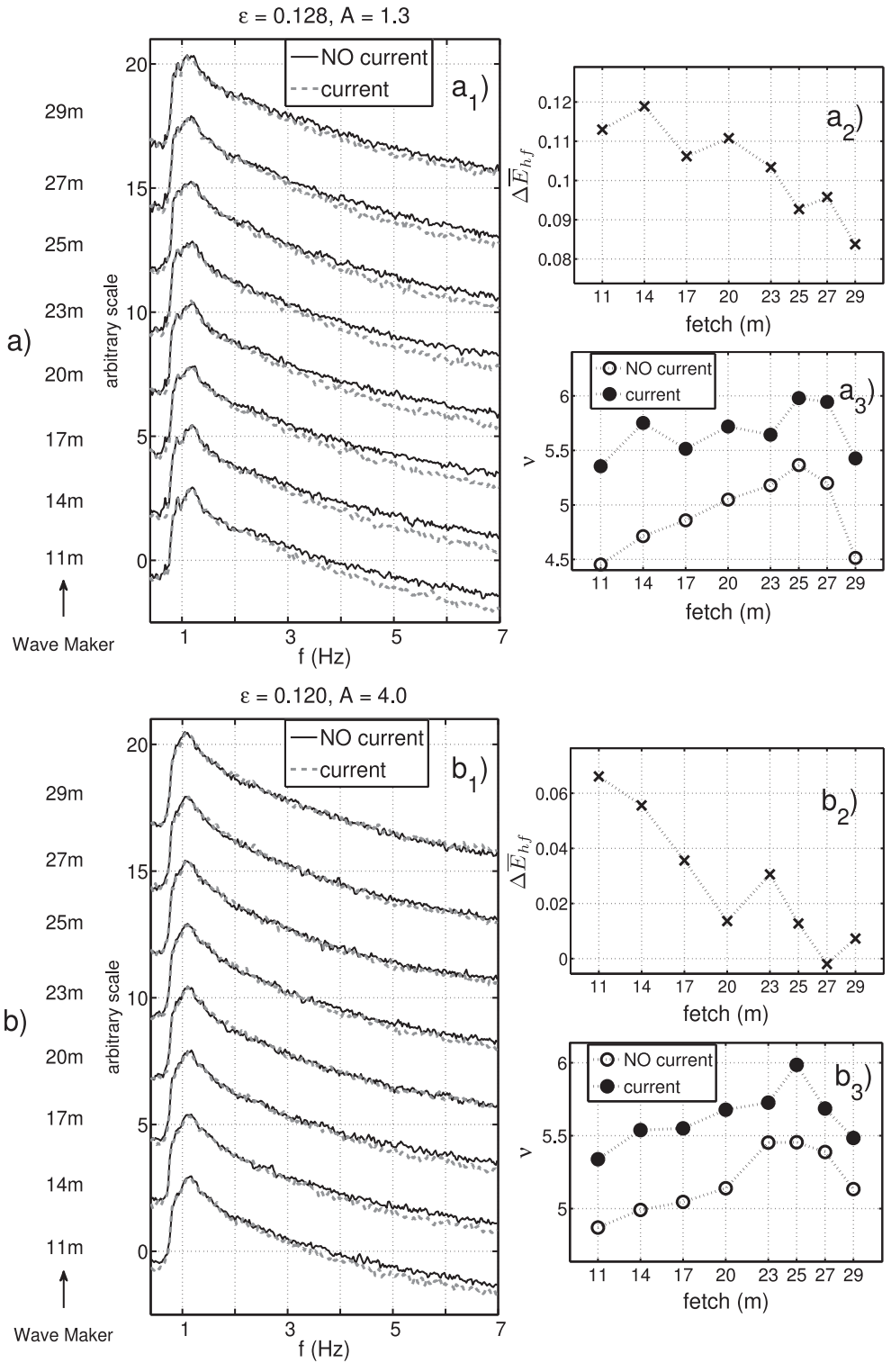

FIG. 9. (a_1),(b_1) Spectral evolution along the fetch for the directionally (a) broadest and (b) narrowest cases. (a_2),(b_2) Evolution of normalized high-frequency energy difference $\Delta\overline{E}_{\mathrm{hf}}$ and (a_3),(b_3) exponent of tail decay ν.

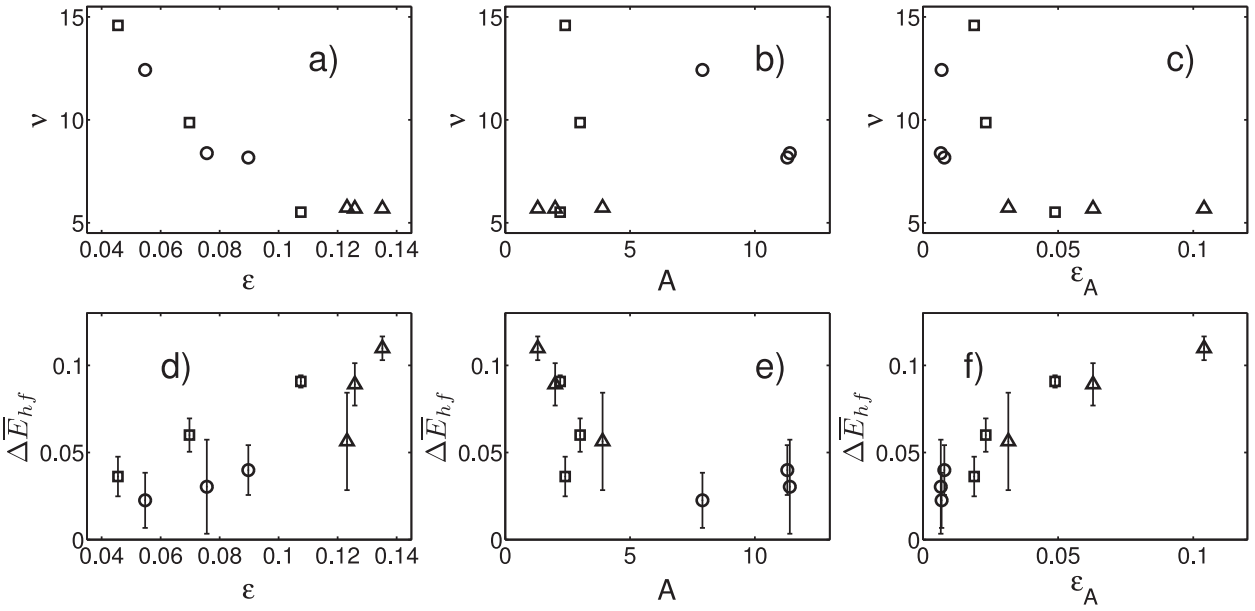

FIG. 10. Relations of steepness ε, parameter A, and parameter ε_A defined in (13) with decay exponent of the high-frequency spectral tail ν and normalized energy difference in the presence and absence of currents $\Delta\overline{E}_{\rm hf}$, as defined in (12): (a) ε vs ν; (b) A vs ν; (c) ε_A vs ν; (d) ε vs $\Delta\overline{E}_{\rm hf}$, (e) A vs $\Delta\overline{E}_{\rm hf}$, and (f) ε_A vs $\Delta\overline{E}_{\rm hf}$. Results correspond to mean values of gauges 2–5 (standard deviation bars shown). Different symbols show irregular wave groups: 2 (varying γ, circles), 3 (varying α, squares), and 4 (varying A, triangles).

always limited ($\Delta\overline{E}_{\rm hf} < 0.3$), including high steepness waves. This explains two features observed. First, there are two distinct evolution curves for the dependence of $\Delta\overline{E}_{\rm hf}$ on the steepness ε (Fig. 10d): one for narrow wave fields (including the unidirectional group, represented by circles and one case of group 4, plotted by a triangle) and another curve for directionally broad spectra (all the other markers). Second, we can see an isolated point of high steepness ($\varepsilon > 0.12$) but at which $\Delta\overline{E}_{\rm hf}$ was relatively low. This case corresponds to the narrowest case of group 4, where the initial waves are steep with directionally confined energy distribution ($A = 4.0$); thus, the spectral evolution is controlled by quasi-resonant interactions. Despite the high steepness and a tail decay close to the power of -5, the current does not suppress the energy cascading process as intensely as for those broader cases, where exact resonances play a fundamental role.

Another interesting characteristic between directionally broad and narrow fields is noticed when we look at the standard deviation of $\Delta\overline{E}_{\rm hf}$ (vertical bars) among the gauges considered in Fig. 10. As shown in Fig. 9, the values of $\Delta\overline{E}_{\rm hf}$ rapidly decrease along the fetch for the case $A = 4.0$. From Fig. 10e, it is observed that the high standard deviations (vertical bars) are predominantly related to directionally confined energy, which is a consequence of the rapid decrease of $\Delta\overline{E}_{\rm hf}$ along the initial sensors of the fetch.

By weighting the steepness with parameter A [(13)], the balance of quasi resonances and exact resonances is included, and the effect of the current-induced detuning is thus better represented (Fig. 10f). However, some of the narrowest cases (unidirectional wave fields, plotted by circles) are ''overweighted'' by their high A values and, within the unidirectional cases (group 2), the dependence is lost. To properly represent the weight of the directional parameter A, a correction is introduced into parameter ε_A based on the argument that directionally narrow wave fields with A above a certain threshold must be weighted equally, that is,

$$\varepsilon_A = \frac{\varepsilon}{A_n}, \quad \text{where} \quad \begin{cases} A_n = A, & \text{if} \quad A < A_{\rm thr} \\ A_n = A_{\rm thr}, & \text{if} \quad A \geq A_{\rm thr} \end{cases}. \tag{14}$$

The use of parameter A_n considers any value of A above a certain threshold $A_{\rm thr}$ as having the same weight on parameter ε_A and therefore the same impact on the current-induced detuning of resonance conditions. Following our arguments that detuning of the quadrilateral conditions are more effective in cases controlled by exact resonances, the threshold $A_{\rm thr}$ would then determine the transition between the predominance of resonant and quasi-resonant interactions. Waseda et al. (2009b), based on the analysis of spectral downshifting and kurtosis, suggested that a value of A around 4 is the transition from the predominance of the exact resonance to

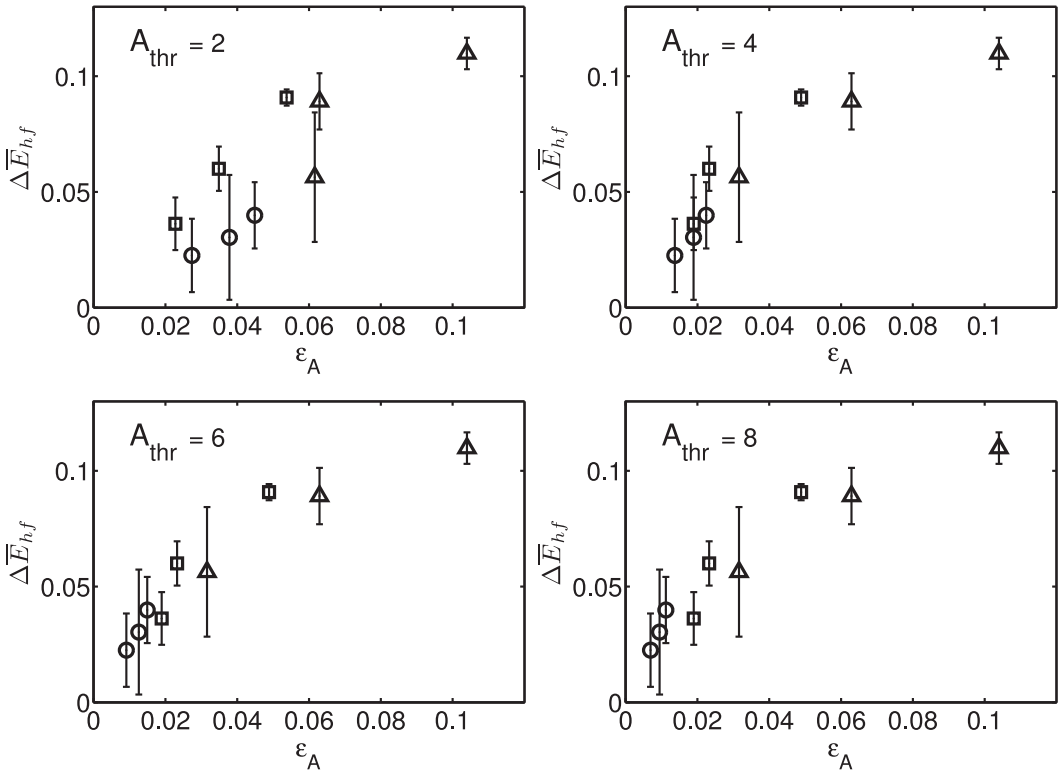

FIG. 11. Relation between parameters ε_A, as defined in (14), and the integrated energy difference in the absence and presence of current $\Delta\overline{E}_{\rm hf}$. Each plot shows a different threshold value $A_{\rm thr}$ applied in (14), as indicated: 2, 4, 6, and 8.

quasi resonance in the nonlinear energy transfer. To verify this hypothesis, we test different threshold values in the new parameter ε_A.

Figure 11 shows the relation of $\Delta\overline{E}_{\rm hf}$ with the new parameter ε_A from (14) with $A_{\rm thr} = 2$, 4, 6, and 8. The range would thus include the limit proposed by Waseda et al. (2009b). We show only these four threshold values; however, all values in the range 1.3–11.3 (minimum and maximum A from our cases) were tested. It is clear that a low threshold around 2 does not unify the distinct curves corresponding to narrow and broad distributions. Values around 8 or above fall in the limitations discussed above, that is, the threshold is too high and overweights the unidirectional cases (circles). It is observed that the best fit that unifies all the A values in a single relation would lie in the range 4–7. No visible differences are seen for $A_{\rm thr}$ values adopted in this range, and they all show a high correlation between ε_A and $\Delta\overline{E}_{\rm hf}$ (>0.9). A value close to 4, as suggested by Waseda et al. (2009b), is the minimum value for which parameter $\Delta\overline{E}_{\rm hf}$ highly correlates to ε_A.

d. *Current-induced broadening of directional spreading*

There is a lack of observations regarding the transformation of the wave directional spectrum under the influence of currents, with the notable exception of Toffoli et al. (2011). In this section, the results of the observed current-induced changes in the directional spectrum and, especially, in the directional spreading are shown.

By analyzing the spreading parameter A, it is observed that practically all initial spectra are considerably broadened in the presence of currents, which is more evident in the narrower cases. Cases with an initial broad spreading (i.e., $A < 2$) showed little changes, although perturbations of the directional spectrum can be seen. Toffoli et al. (2011) also observed broadening of the directional spreading of waves propagating over an oblique current field. Two examples are shown in Fig. 12. The spectra of the narrowest and broadest cases (top and bottom panels, respectively) of the varying spreading group (group 4) are plotted in the absence and presence of currents (left- and right-hand columns, respectively).

The systematic broadening observed is suggested to be related to the high spatial and temporal variability of the current field in the tank, which would randomly refract the wave rays with a consequent scattering of wave energy. This process is comparable to wave propagation over intermediate to shallow water depths. Scattering of waves by irregular bottom topography was first

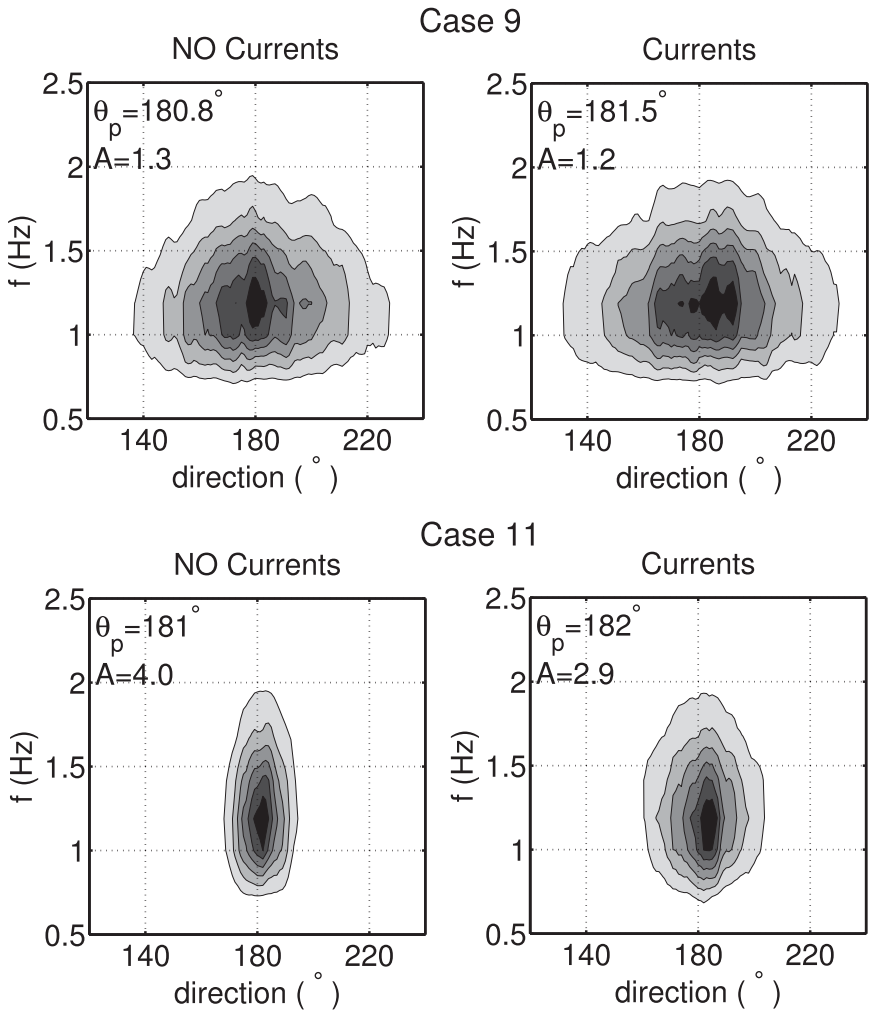

FIG. 12. Directional spectra for the (top) broadest (case 9) and (bottom) narrowest (case 11) directional spreading cases of group 3. Spectra (left) are in the absence of currents and (right) with a background current field. Parameters A and θ_p are shown for each plot.

investigated by Long (1973). Additionally, Ardhuin et al. (2003) implemented a numerical Eulerian–Lagrangian model to account for wave ray refraction over small-scale bottom features. From data analysis along the continental shelf, they observed that the distribution of wave energy was broadened in direction, particularly for directionally narrow swells at the inner shelf. The broadening was associated with the scatter of wave rays due to small-scale bottom topography and agreed with predictions from their Bragg scattering model. We believe a similar process occurs when waves propagate over a variable current field, which is observed from our results. Waves are scattered in random directions due to the highly variable current field. The wavenumbers also change in time due to the unsteadiness of the current field. This results in variations of the direction of propagation of each component with a consequent broadening pattern of the final spectrum.

The difference of parameter A in the absence and presence of currents is shown in Fig. 13 against the initial A (i.e., A in the absence of currents) for all irregular wave experiments; ΔA represents the difference $A_{\mathrm{NOcurr}} - A_{\mathrm{curr}}$. Figure 13b shows changes in peak direction ($\Delta\theta_p$). The predominant direction in which the energy propagates shows no relation with the initial directional spreading. The spatial distribution of the currents is modified along the time, and it produces different values of $\Delta\theta_p$. It was observed that the refraction of the main energy peak is considerably less intense than it is for regular waves. However, the directional spreading exhibits an evident broadening pattern. Since the spectral shape of a narrow, initial spectra (i.e., $A > 3$) is subject to more drastic changes, the broadening is more evident for narrower cases and consequently ΔA highly correlates to the initial value of A.

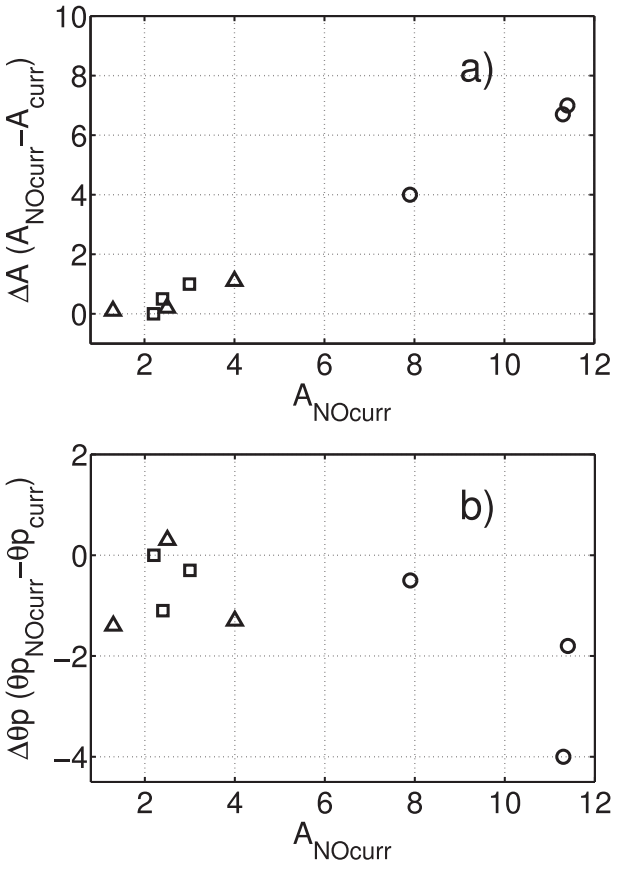

FIG. 13. Variation of parameter A and peak direction θ_p in the absence and presence of currents as a function of A in the absence of currents (A_{NOcurr}): (a) $\Delta A = A_{\mathrm{NOcurr}} - A_{\mathrm{curr}}$ and (b) $\Delta\theta_p = \theta_{p\mathrm{NOcurr}} - \theta_{p\mathrm{curr}}$. Different symbols show irregular wave groups: 2 (varying γ, circles), 3 (varying α, squares), and 4 (varying A, triangles).

To complement our analysis, we use some of the results of the experiments performed and presented in Toffoli et al. (2015) and Waseda et al. (2015); five different opposing current fields are generated with increasing mean speed, from which the obtained mean values are $U = -4.13$, -5.99, -10.48, and $-13.39\,\mathrm{cm\,s^{-1}}$. The initial wave field, in the absence of currents, is represented by $T_p = 0.871$, $\varepsilon = 0.095$, and $A = 3.3$. The directional distribution is considerably narrow, and the broadening is expected to be evident. The purpose of analyzing only additional opposing current cases is to complement our results, where coflowing currents were investigated. Therefore, we can verify if the broadening occurs regardless of the mean current direction.

Waseda et al. (2015) show that the currents are more unsteady as the mean velocity increases. The spatial distribution of the current field is expected to be less homogeneous. According to our assumptions of wave rays scattering, as the standard deviation of the currents increases, the directional broadening of the wave spectrum would be expected to be more intense. This is exactly what we see from the additional results (Fig. 14). The directional spectra are shown in the top panels (including for $U = 0$). In the bottom panels, the measured directional spreading parameter A is plotted against the mean (left-hand side) and standard deviation (right-hand side) of the time series of the current speed. The broadening of the directional distribution in the presence of currents is evident. Since the variability of the current increases for higher mean speed fields (Waseda et al. 2015), parameter A is inversely proportional to the mean and standard deviation of the currents. We can also see that the spectral energy in high frequencies is progressively suppressed as the current standard deviation (and mean speed) increases, which was also observed by Waseda et al. (2015) through the analysis of the 1D spectra.

Therefore, the broadening and suppression of high-frequency energy occur for coflowing as well as opposing currents. The main factor is how variable and unstable the background current field is and not a direct consequence of the Doppler effect. The random refraction and scattering of wave components result in the final broadening of the directional spectrum. If the wavenumbers are randomly refracted and the energetic part of the spectrum is perturbed in time, the energy transfer to high frequencies and the maintenance of a high-frequency spectral tail are suppressed. A remaining question is whether this perturbation prevails in space and time, that is, whether wave interactions would act in a way to restore the equilibrium spectral shape under the broadening force at longer space–time scales, and more tests and observations are needed to investigate this balance.

5. Conclusions

This study investigates the effects of a highly variable current field on the spectral shape of propagating waves. Despite the spatiotemporal variability of the currents in the tank, some patterns in the wave spectrum are observed, which are mainly concerned with the suppression of energy cascading to higher frequencies and directional broadening.

The main current-induced effects on single wave trains are related to random directional changes, which consequently modulate wave height. The spatial structure of the current field is variable, and consequently the refraction patterns are modified for each experiment. The presence of currents has no influence on the wave absolute frequency, which suggests that a stationary or slow-varying current approximation holds.

Having the previous background results for monochromatic waves, our analysis of irregular waves was

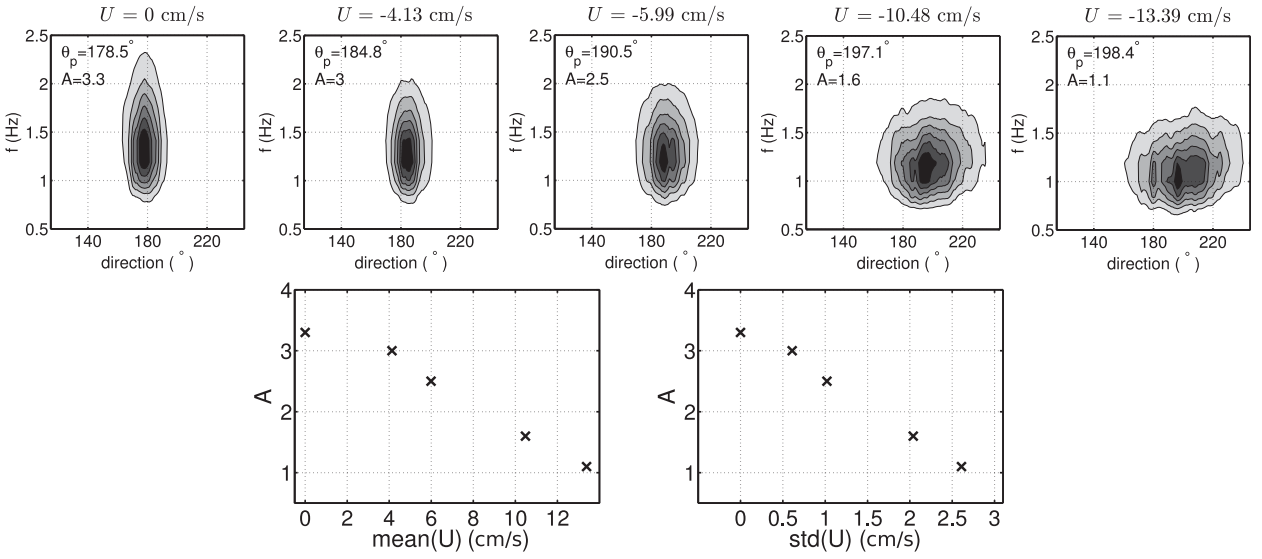

FIG. 14. (top) Directional spectra for the same initial wave signal and varying opposing current field and (bottom) directional spreading parameter A as a function of the mean current speed and standard deviation (left- and right-hand sides, respectively).

focused on the spectral geometry only. In the absence of currents, a progressive downshifting of the spectral peak along the fetch is observed. Unlike the regular wave cases, the peak frequency is changed under the influence of currents, and the downshifting of the peak, represented by the ratio between the peak frequency in advanced and early stages, is reduced. This result indicates that the nonlinear interactions responsible for downshifting the spectral peak are perturbed when currents are present.

The wave energy is transferred to frequencies beyond the generated wave frequencies via wave–wave energy exchanges. This process offers a valuable opportunity to study current-induced effects on the nonlinear interactions. The investigation of unidirectional and directional irregular waves shows that the interaction between wave components is more intense as the spectral steepness increases. In the presence of currents, the energy transfer to higher frequencies beyond the wavemaker upper limit is suppressed, which can be explained by the detuning of the four-wave resonant conditions, proposed by Waseda et al. (2015). To quantify this process, we calculate the integrated normalized energy difference in high frequencies between current and no current spectra $\Delta\overline{E}_{\mathrm{hf}}$. The high-frequency energy suppression is more intense for steeper waves and, interestingly, broader directional spreading. Therefore, parameter $\Delta\overline{E}_{\mathrm{hf}}$ shows to be a function of the initial spectral steepness ε, but it is limited when the spectrum is sufficiently narrow. By introducing a new parameter ε_A, which relates the steepness to the inverse normalized directional distribution A, we found that the relation of $\Delta\overline{E}_{\mathrm{hf}}$ better correlates with ε_A.

If the steepness is high enough and the directional spectrum is sufficiently broad, exact resonances are the main mechanism of wave energy exchanges and maintenance of a high-frequency tail. The results suggest that, for these cases, the random current field is more effective in detuning the four-wave interaction conditions than for waves with directionally confined energy, where quasi-resonant interactions are predominant. The detuning force seems to not prevail along the fetch and the tail tends to an equilibrium as the waves propagate, which occurs more rapidly for the directionally narrow waves. Therefore, parameter ε_A is an attempt to include the physics observed from our findings that the detuning of resonance conditions caused by the background current is more effective when the spectral evolution is controlled by exact resonances (broad directional distribution) over quasi resonances (directionally confined energy distribution). Furthermore, it was observed that a threshold for A must be included in ε_A, which would represent the switch between exact and quasi resonances. Thus, any value of A above the applied threshold assumes the same value. For an observed threshold in the range 4–7, $\Delta\overline{E}_{\mathrm{hf}}$ highly correlates with ε_A.

The impact of the random current field extends to the directional distribution of wave energy. Random refraction scatters the wave energy and a consequent broadening of the directional spreading occurs. All the experimental cases showed broadening of the observed wave spectrum, except for one of the broadest case. As the directional spectrum narrows, the current-induced broadening is more evident. Additional results with opposing current fields also show that the broadening is

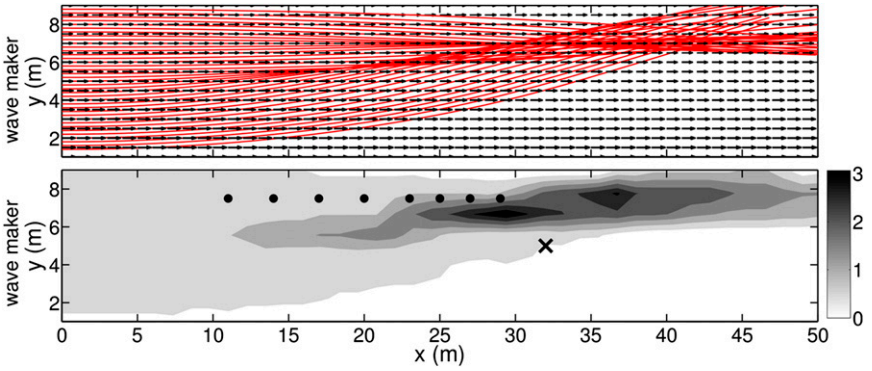

FIG. A1. Simulation of wave ray trajectories using the mean current speed values of Table 1. (top) Current vectors and ray paths (red lines); (bottom) relative changes in the number of rays and position of sensors, where circles represent the wave gauges in the linear array, and the "x" marker shows the location where the directional spectrum is obtained.

intensified as the standard deviation of the current increases. Therefore, the broadening effect is not related to the direction of the current relative to the wave propagation but instead to the spatiotemporal variability of the current field. It is suggested that the mechanism behind this process is similar to wave ray scattering over small-scale variable bottom features (Long 1973), which is related to broadening of the directional spreading of waves approaching coastal waters (Ardhuin et al. 2003). The disturbance of wavenumbers caused by wave refraction thus weakens the nonlinear interactions by detuning the resonant conditions, and consequently the energy inflow into shorter waves is suppressed.

Acknowledgments. We thank the support and assistance of Mr. Itakura and Kent Mozumbi during the experiments in the University of Tokyo wave tank. We are thankful to Amin Chabchoub for the advice and help on the experimental setup. The support of ONR Grant N000141310278 and of the Australian Research Council through Discovery Grant DP130100227 is acknowledged by A.V.B.; T.W. and A.T acknowledge support from the JSPS Fellowship for Research in Japan Program, Grants-in-Aid for Scientific Research of the JSPS, and the International Science Linkages (ISL) Program of the Australian Academy of Science. The first author is thankful for support from the Australian Victorian Government through the Victorian International Research Scholarship.

APPENDIX

Focusing/Defocusing of Wave Energy Induced by the Currents in the Tank

The quantification of the observed spectral modifications based on the arguments of focusing/defocusing of wave energy is a complicated task. Since the currents in the tank are highly variable in space and time, the induced refraction pattern becomes extremely hard to reproduce. However, one possibility is to consider the statistics shown in Table 1. The mean current speed at

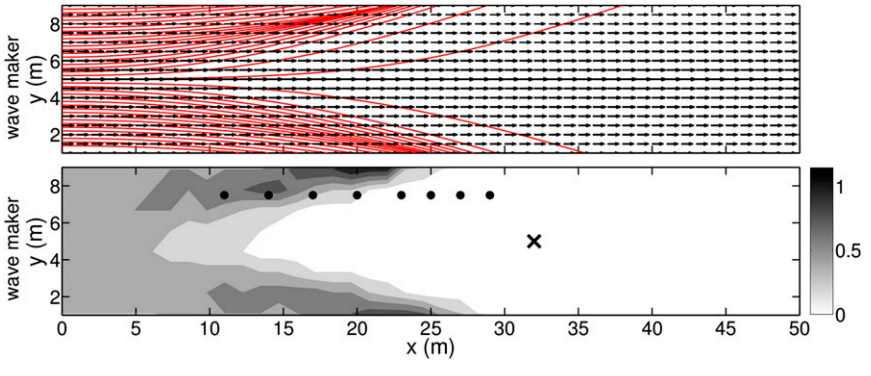

FIG. A2. Same ray diagram and estimated focusing/defocusing of rays as in Fig. A1 but considering different values for the current speed at positions R2–L2.

the five positions suggests that the gradient is variable along the cross section. The ray trajectories can be numerically simulated through the geometrical optics approximation (e.g., Kenyon 1971) and considering the values of Table 1 constant along the tank. This approach can provide an average refraction pattern. We can estimate the degree of convergence using a straightforward method proposed in Rapizo et al. (2014) based on ray counting. This method is applied for an incoming number of 300 rays, which provides a reasonable estimation of the degree of convergence eventually induced by the mean current profile. Figure A1 shows the ray-tracing simulation (top panel). The bottom panel shows the focusing/defocusing of rays in relation to the original incoming number of rays per grid cell, which was made by dividing the grid in 1 m × 1 m cells.

Although Fig. A1 provides a sense of the intensity of energy focusing/defocusing in the tank, it is a rough estimation and can be misleading. First, the current field is not homogeneous in the along-channel direction (Takahashi 2011; Toffoli et al. 2013). Second, the variability of the current on the right-hand side can reach 40% of the mean value, while the current on the left side is comparatively steady. Despite the lower mean value of 8 cm s^{-1} at position L2, the values at positions R2 and R1, for example, reach lower values than 8 cm s^{-1} (see Fig. 2). This would make the gradient vectors completely inverse their direction and change the refraction patterns along the time. As a consequence, the region where the energy converges can experience a divergence of wave rays at other times. The reason for the variation of wave energy over the sensors in the pentagon for different experiments in the presence of currents is probably associated with the variability of focusing/defocusing patterns. To exemplify this process, Fig. A2 shows the same ray diagram of Fig. A1, but considering a different and possible distribution of the current field due to its variability, based on measured values. The rays now strongly diverge from the center. This estimation again considers a velocity field constant along the tank. It is important to stress that Figs. A1 and A2 are potential snapshots only and not meant to be predictive. Therefore, the spatiotemporal variability of the current field is significant and thus treated in the present study as random.

Finally, we can have an estimation of focusing/defocusing by analyzing the time series of surface elevation of a regular wave. Figure A3 shows an example of a time series recorded in the absence (black line) and presence (blue line) of currents. In the presence of currents, the amplitude varies considerably and can be reduced by 35% and increased by 30% compared with conditions of $U = 0$. The modulation of the wave on currents is rather random and, based on the aforementioned argument, likely to be associated with refraction induced by the current field.

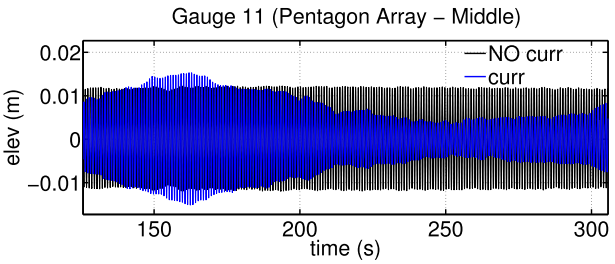

FIG. A3. Comparison of time series of surface elevation in the presence (blue) and absence (black) of currents for the regular wave case 1 (gauge 11).

REFERENCES

Annenkov, S. Y., and V. I. Shrira, 2006: Role of non-resonant interactions in the evolution of nonlinear random water wave fields. *J. Fluid Mech.*, **561**, 181–207, doi:10.1017/S0022112006000632.

Ardhuin, F., W. C. O'Reilly, T. H. C. Herbers, and P. F. Jessen, 2003: Swell transformation across the continental shelf. Part I: Attenuation and directional broadening. *J. Phys. Oceanogr.*, **33**, 1921–1939, doi:10.1175/1520-0485(2003)033<1921:STATCS>2.0.CO;2.

——, and Coauthors, 2012: Numerical wave modeling in conditions with strong currents: Dissipation, refraction, and relative wind. *J. Phys. Oceanogr.*, **42**, 2101–2120, doi:10.1175/JPO-D-11-0220.1.

Babanin, A. V., and Y. P. Soloviev, 1998: Variability of directional spectra of wind-generated waves, studied by means of wave staff arrays. *Mar. Freshwater Res.*, **49**, 89–101, doi:10.1071/MF96126.

——, H. Hwung, I. Shugan, A. Roland, A. V. der Westhuysen, A. Chawla, and C. Gautier, 2011: Nonlinear waves on collinear currents with horizontal velocity gradient. *Proc. 12th Int. Workshop on Wave Hindcasting and Forecasting and Third Coastal Hazards Symp.*, Kohala Coast, Hawaii, Wave Workshop, 1–24. [Available online at http://www.waveworkshop.org/12thWaves/papers/Babanin_et_al_2011_Hawaii_submitted.pdf.]

Benjamin, T. B., and J. E. Feir, 1967: The disintegration of wave trains on deep water. Part 1. Theory. *J. Fluid Mech.*, **27**, 417–430, doi:10.1017/S002211206700045X.

Benney, D. J., 1962: Non-linear gravity wave interactions. *J. Fluid Mech.*, **14**, 577–584, doi:10.1017/S0022112062001469.

Chawla, A., and J. T. Kirby, 2002: Monochromatic and random wave breaking at blocking points. *J. Geophys. Res.*, **107**, doi:10.1029/2001JC001042.

Donelan, M., W. M. Drennan, and A. K. Magnusson, 1996: Nonstationary analysis of the directional properties of propagating waves. *J. Phys. Oceanogr.*, **26**, 1901–1914, doi:10.1175/1520-0485(1996)026<1901:NAOTDP>2.0.CO;2.

Gramstad, O., and A. V. Babanin, 2016: The generalized kinetic equation as a model for the nonlinear transfer in third-generation wave models. *Ocean Dyn.*, **66**, 509–526, doi:10.1007/s10236-016-0940-4.

Hasselmann, K., 1962: On the non-linear energy transfer in a gravity-wave spectrum. Part 1. General theory. *J. Fluid Mech.*, **12**, 481–500, doi:10.1017/S0022112062000373.

——, and Coauthors, 1973: Measurements of wind-wave growth and swell decay during the Joint North Sea Waves Project

(JONSWAP). Ergänzungsheft zur Deutschen Hydrographischen Zeitschrift 12, 95 pp.

Haus, B. K., 2007: Surface current effects on the fetch-limited growth of wave energy. *J. Geophys. Res.*, **112**, C03003, doi:10.1029/2006JC003924.

Janssen, P. A. E. M., 2003: Nonlinear four-wave interactions and freak waves. *J. Phys. Oceanogr.*, **33**, 863–884, doi:10.1175/1520-0485(2003)33<863:NFIAFW>2.0.CO;2.

Kenyon, K. E., 1971: Wave refraction in ocean currents. *Deep-Sea Res. Oceanogr. Abstr.*, **18**, 1023–1034, doi:10.1016/0011-7471(71)90006-4.

Krasitskii, V. P., 1994: On reduced equations in the Hamiltonian theory of weakly nonlinear surface waves. *J. Fluid Mech.*, **272**, 1–20, doi:10.1017/S0022112094004350.

Lai, R. J., S. R. Long, and N. E. Huang, 1989: Laboratory studies of wave-current interaction: Kinematics of the strong interaction. *J. Geophys. Res.*, **94**, 16 201–16 214, doi:10.1029/JC094iC11p16201.

Long, R. B., 1973: Scattering surface of waves an irregular by bottom. *J. Geophys. Res.*, **78**, 7861–7870, doi:10.1029/JC078i033p07861.

Longuet-Higgins, M. S., 1962: Resonant interactions between two trains of gravity waves. *J. Fluid Mech.*, **12**, 321–332, doi:10.1017/S0022112062000233.

——, and R. W. Stewart, 1961: The changes in amplitude of short gravity waves on steady non-uniform currents. *J. Fluid Mech.*, **10**, 529–549, doi:10.1017/S0022112061000342.

——, and O. M. Phillips, 1962: Phase velocity effects in tertiary wave-interactions. *J. Fluid Mech.*, **12**, 333–336, doi:10.1017/S0022112062000245.

Mitsuyasu, H., F. Tasai, T. Suhara, S. Mizuno, M. Ohkusu, T. Honda, and K. Rikiishi, 1975: Observations of the directional spectrum of ocean waves using a cloverleaf buoy. *J. Phys. Oceanogr.*, **5**, 750–759, doi:10.1175/1520-0485(1975)005<0750:OOTDSO>2.0.CO;2.

Moreira, R. M., and D. H. Peregrine, 2012: Nonlinear interactions between deep-water waves and currents. *J. Fluid Mech.*, **691**, 1–25, doi:10.1017/jfm.2011.436.

Mori, N., M. Onorato, and P. A. E. M. Jansen, 2011: On the estimation of the kurtosis in directional sea states for freak wave forecasting. *J. Phys. Oceanogr.*, **41**, 1484–1497, doi:10.1175/2011JPO4542.1.

Onorato, M., A. Osborne, M. Serio, L. Cavaleri, C. Brandini, and C. Stansberg, 2004: Observation of strongly non-Gaussian statistics for random sea surface gravity waves in wave flume experiments. *Phys. Rev.*, **70**, 067302, doi:10.1103/PhysRevE.70.067302.

——, D. Proment, and A. Toffoli, 2011: Triggering rogue waves in opposing currents. *Phys. Rev. Lett.*, **107**, 184502, doi:10.1103/PhysRevLett.107.184502.

Phillips, O. M., 1960: On the dynamics of unsteady gravity waves of finite amplitude. Part 1. The elementary interactions. *J. Fluid Mech.*, **9**, 193–217, doi:10.1017/S0022112060001043.

——, 1977: *The Dynamics of the Upper Ocean*. Cambridge University Press, 336 pp.

Qingpu, Z., 1996: Nonlinear instability of wavetrain under influences of shear current with varying vorticity and air pressure. *Acta Mech. Sin.*, **12**, 24–38, doi:10.1007/BF02486759.

Rapizo, H., A. Babanin, O. Gramstad, and M. Ghantous, 2014: Wave refraction on Southern Ocean eddies. *Proc. 19th Australasian Fluid Mechanics Conf.*, Melbourne, Australia, Australian Fluid Mechanics Society, 1–4. [Available online at http://people.eng.unimelb.edu.au/imarusic/proceedings/19/18.pdf.]

Ribal, A., A. V. Babanin, I. R. Young, A. Toffoli, and M. Stiassnie, 2013: Recurrent solutions of the Alber equation initialized by Joint North Sea Wave Project spectra. *J. Fluid Mech.*, **719**, 314–344, doi:10.1017/jfm.2013.7.

Stewart, R. H., and J. W. Joy, 1974: HF radio measurements of surface currents. *Deep-Sea Res. Oceanogr. Abstr.*, **21**, 1039–1049, doi:10.1016/0011-7471(74)90066-7.

Takahashi, S., 2011: Particle motions of nonlinear water waves (in Japanese). M.S. thesis, University of Tokyo, Graduate School of Frontier Sciences, Japan, 83 pp.

Tamura, H., T. Waseda, Y. Miyazawa, and K. Komatsu, 2008: Current-induced modulation of the ocean wave spectrum and the role of nonlinear energy transfer. *J. Phys. Oceanogr.*, **38**, 2662–2684, doi:10.1175/2008JPO4000.1.

Tanaka, M., 2001: Verification of Hasselmann's energy transfer among surface gravity waves by direct numerical simulations of primitive equations. *J. Fluid Mech.*, **444**, 199–221, doi:10.1017/S0022112001005389.

Toffoli, A., and Coauthors, 2011: Occurrence of extreme waves in three-dimensional mechanically generated wave fields propagating over an oblique current. *Nat. Hazards Earth Syst. Sci.*, **11**, 895–903, doi:10.5194/nhess-11-895-2011.

——, T. Waseda, H. Houtani, T. Kinoshita, K. Collins, D. Proment, and M. Onorato, 2013: Excitation of rogue waves in a variable medium: An experimental study on the interaction of water waves and currents. *Phys. Rev.*, **87**, 051201, doi:10.1103/PhysRevE.87.051201.

——, ——, ——, L. Caveleri, D. Greaves, and M. Onorato, 2015: Rogue waves in opposing currents: An experimental study on deterministic and stochastic wave trains. *J. Fluid Mech.*, **769**, 277–297, doi:10.1017/jfm.2015.132.

Trulsen, G. N., K. B. Dysthe, and J. Trulsen, 1990: Evolution of a gravity wave spectrum through a current gradient. *J. Geophys. Res.*, **95**, 22 141–22 151, doi:10.1029/JC095iC12p22141.

Waseda, T., T. Kinoshita, and H. Tamura, 2009a: Evolution of a random directional wave and freak wave occurrence. *J. Phys. Oceanogr.*, **39**, 621–639, doi:10.1175/2008JPO4031.1.

——, ——, and ——, 2009b: Interplay of resonant and quasi-resonant interaction of the directional ocean waves. *J. Phys. Oceanogr.*, **39**, 2351–2362, doi:10.1175/2009JPO4147.1.

——, ——, L. Cavaleri, and A. Toffoli, 2015: Third-order resonant wave interactions under the influence of background current fields. *J. Fluid Mech.*, **784**, 51–73, doi:10.1017/jfm.2015.578.

White, B., and B. Fornberg, 1998: On the chance of freak waves at sea. *J. Fluid Mech.*, **355**, 113–138, doi:10.1017/S0022112097007751.

Young, I. R., and G. Van Vleder, 1993: A review of the central role of nonlinear interactions in wind–wave evolution. *Philos. Trans. Roy. Soc. London*, **342**, 505–524, doi:10.1098/rsta.1993.0030.

Yuen, H. C., and W. E. Ferguson, 1982: Nonlinear dynamics of deep-water gravity waves. *Adv. Appl. Mech.*, **22**, 67–229, doi:10.1016/S0065-2156(08)70066-8.

Zakharov, V. E., 1968: Stability of periodic waves of finite amplitude on the surface of a deep fluid. *J. Appl. Mech. Tech. Phys.*, **9**, 190–194, doi:10.1007/BF00913182.